Transcription-dependent domain-scale three-dimensional genome organization in the dinoflagellate *Breviolum minutum*

Georgi K. Marinov[1,*,#], Alexandro E. Trevino[3,7,*], Tingting Xiang[2,8,*], Anshul Kundaje[1,6], Arthur R. Grossman[2], and William J. Greenleaf[1,3,4,5,#]

[1] *Department of Genetics, Stanford University, Stanford, California 94305, USA*
[2] *Carnegie Institution for Science, Department of Plant Biology, Stanford, California 94305, USA*
[3] *Center for Personal Dynamic Regulomes, Stanford University, Stanford, California 94305, USA*
[4] *Department of Applied Physics, Stanford University, Stanford, California 94305, USA*
[5] *Chan Zuckerberg Biohub, San Francisco, California, USA*
[6] *Department of Computer Science, Stanford University, Stanford, California 94305, USA*
[7] *Department of Bioengineering, Stanford University, Stanford, California 94305, USA*
[8] *Department of Biological Sciences, University of North Carolina at Charlotte, Charlotte, NC 28223, USA*
[*] *These authors contributed equally to this work*
[#] *Corresponding author*

Abstract

Dinoflagellate chromosomes represent a unique evolutionary experiment, as they exist in a permanently condensed, liquid crystalline state, are not packaged by histones, and contain genes organized into tandem gene arrays, with minimal transcriptional regulation. We analyze the three-dimensional (3D) genome of *Breviolum minutum*, and find large topological domains ("dinoTADs") without chromatin loops, which are demarcated by convergent gene array boundaries. Transcriptional inhibition disrupts dinoTADs, implicating transcription-induced supercoiling as the primary topological force in dinoflagellates.

The three-dimensional (3D) genome architecture of cells has functional consequences for gene regulation, organismal development, DNA replication, and mutational processes. Topologically associating domains (TADs) and compartments on the sub-megabase scale are conserved architectural features of eukaryote genomes, defined by increased intradomain contact frequencies and interdomain contact insulation[2]. Mechanisms known to drive the folding of such domains include constraints on cohesin-mediated loop extrusion – imposed in part by CTCF in vertebrates – and self-associations between similar chromatin states[3]. Other mechanisms, including insulation of domains by polymerases or specific boundary proteins, have also been proposed to play roles in genome architecture[4]. However, the extent to which genome function may influence genome folding, for example through transcriptional activity, is poorly understood. There has also been little exploration of 3D organization across eukaryotes, even though major deviations from conventional norms are known to exist, presenting natural experiments that may reveal deeper underlying organizational principles masked in other lineages.

Dinoflagellates are the most radical such departure. They are a diverse, widespread clade playing major roles in aquatic ecosystems, for example, as symbionts of corals, providing the metabolic basis for reef ecosystems. Dinoflagellates possess numerous highly divergent molecular features[5], including, uniquely among eukaryotes, the loss of nucleosomal packaging of chromatin. Histones are extremely conserved across eukaryotes, were present in their current form already in the last eukaryotic common ancestor[6], and they and their posttranslational modifications are pivotal to all biochemical processes involving chromatin.

Dinoflagellates are the sole known exception. Their chromosomes exist in a liquid crystalline state, are permanently condensed throughout the cell cycle, and, although highly divergent histone genes are retained in their genomes[7], a combination of virus-derived nucleoproteins and bacterial-derived histone-like proteins have taken over as main packaging components[8]. Dinoflagellate genomes are often huge (up to $\geq$200 Gb), genes are organized into tandem gene arrays, individual mRNAs are generated through *trans*-splicing, and transcriptional regulation is largely absent[8]. These fascinating features simultaneously pose intriguing questions regarding the adaptation of transcriptional and regulatory mechanisms to the absence of nucleosomes, and provide a unique opportunity to explore

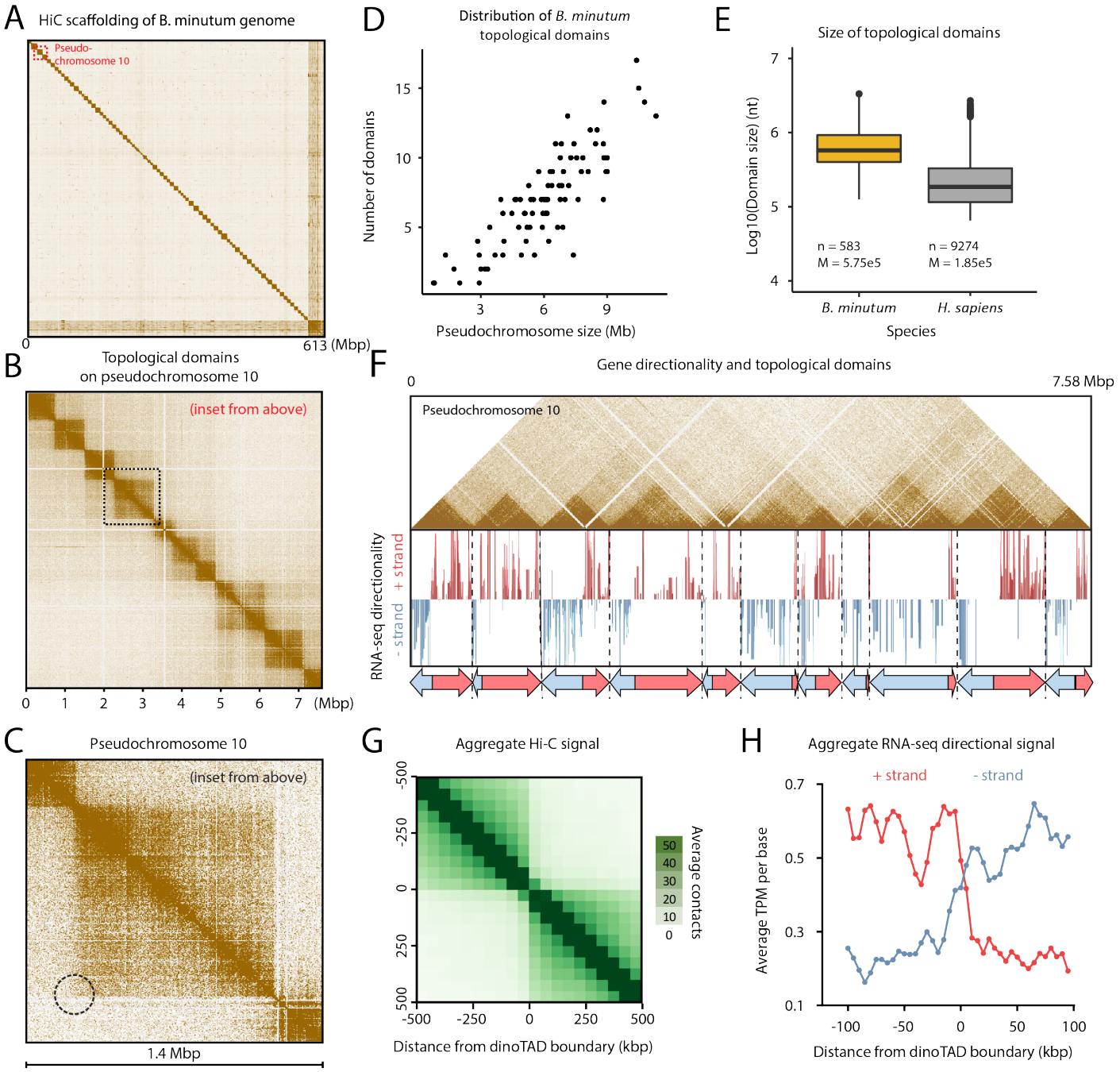

Fig. 1: *B. minutum* genome is physically partitioned into dinoTADs defined by tandem gene arrays. (A) Hi-C scaffolding of the *B. minutum* draft genome assembly. (B) Inset from (A). KR-normalized 5-kb resolution Hi-C map for pseudochromosome 10. (C) Inset from (B). Hi-C loops and stripes are not observed in dinoTADs (dotted circle notes where a loop would be). (D) Scaling of chromosome size with dinoTAD number. (E) Comparison of human and *B. minutum* topological domain sizes. Box plots show the 25th, 50th and 75th percentiles, whiskers show the 5-95% intervals; $n = 583$ for dinoTADs, $n = 9{,}274$ for human TADs. (F) Hi-C map (5-kb resolution) for pseudochromosome 10 together with forward- and reverse-strand transcript levels and gene arrays. (G) Average Hi-C contacts across dinoTAD boundaries (dinoTADs were called at a 50-kb resolution using HiCExplorer [1]; see the Supplementary Methods for details). (H) Average forward- and reverse-strand RNA-seq levels across dinoTAD boundaries.

the biophysical forces underlying genomic organization in the context of a large eukaryotic genome nearly devoid of nucleosomes.

To explore these questions, we applied chromosome con-

formation capture using Hi-C on the coral symbiont *Breviolum minutum*. We generated multiple libraries under standard growth conditions and for cells grown at elevated temperature, obtaining ∼150–220 million Hi-C contacts for each (Supplementary Table 1). We pooled these libraries to generate a chromosome-level scaffolding of the previously fragmented *B. minutum* assembly[9]. We identified 91 major pseudochromosomes (≥ 500 kb), encompassing ∼94% of the total sequence (Fig. 1A-B; Supplementary Fig. 1A), the longest being ∼11 Mbp in size, with a median length of 6.7 Mbp (Supplementary Fig. 1A). At 1-Mbp resolution, they exhibit a bipartite (occasionally tripartite) structure (Supplementary Fig. 2).

Additional untreated libraries (Supplementary Table 1) were combined to generate an even higher-resolution map (∼1.05 billion contacts), which was used to examine fine-scale features of topological organization. High-resolution (5-kb) maps revealed well-defined (comparably so to those observed in mammals) topological domains, ≤200 kb–≥2 Mb in size (Fig. 1B-E; Supplementary Fig. 3–12). In mammals, most TAD boundaries are demarcated by CTCF sites blocking loop extrusion, reflected in Hi-C maps by chromatin loops and "stripes". We observe no loop or stripe features in *B. minutum* (Fig. 1C), suggesting a different mechanism for the formation of dinoflagellate TADs, which we term "dinoTADs". Omitting the denaturation step in the Hi-C protocol, which should better preserve protein-protein contacts strongly accentuated dinoTADs, but still did not reveal signs of loops or loop extrusion domains; Supplementary Fig. 14). Detected dinoTAD number correlates with chromosome size (Fig. 1D), and observed dinoTADs are considerably larger than mammalian TADs (Fig. 1E).

We next compared Hi-C maps to available annotation features. Remarkably, we found that each dinoTAD corresponds to a pair of divergent gene arrays (Fig. 1F), and dinoTAD boundaries coincide with convergence between gene arrays (Fig. 1G-H).

Numerous models for dinoflagellate chromosome organization have been suggested since the 1960s, primarily based on electron microscopy. These include proposals that chromosomes are organized as "toroidal chromonemas"[11], "stacks of discs"[12], "cored pineapples"[13], or around "central core fibers"[14]. Most of these models imply specific topological constraints maintaining the proposed shapes and are not directly reconcilable with our Hi-C observations.

Instead, the correspondence between dinoTADs and gene arrays suggested a role for transcription in their formation. Although TADs form independently of transcription in animal cells, transcription-induced self-interacting domains have been previously demonstrated in bacteria[15], and similar mechanisms have been proposed to explain some topological features in fission yeast[16]. We also note that a handful of models of dinoflagellate chromosome structure have suggested the presence of coil/plectoneme-like features[17,18], but without relating them to gene arrays and transcription. This model is also supported by the observation that frequently each dinoTAD can be divided into more diffuse "sub-dinoTADs" corresponding to the two individual gene arrays in a pair (Fig. 1C; Supplementary Fig. 3–12), which could be the result of torsion generated in each direction of transcription.

The model makes a clear prediction – inhibition of transcription should result in dinoTADs decompaction. To test this relationship, we first compared Hi-C maps for cells grown at 34 °C versus 27 °C, as heat stress could result in general transcription reduction[19]. We observed mild decompaction of dinoTADs at 34 °C, though domains remained intact (Supplementary Fig. 19–21).

We next carried out chemical transcription inhibition experiments. Since transcription inhibition conditions for *B. minutum* are not well established, we chose two inhibitors – triptolide and α-amanitin – with distinct mechanisms of action, and assayed multiple time points and doses (Fig. 2A-B). Amanitin directly inhibits RNA Polymerase II and is slow acting, while triptolide quickly blocks initiation by targeting the TFIIH XPB subunit[20]. While dinoflagellate RNA polymerase II has been reported to be sensitive to α-amanitin, it is possible that the sensitivity is somewhat partial[21]; in addition, the *B. minutum* XPB homolog is highly divergent[9], thus a moderate inhibition effect is not unexpected. We therefore carried out several experiments to directly estimate the extent of transcription inhibition. Direct metabolic labeling approaches[22] were unsuccessful as it appears that Symbiodiniaceae cells are impermeable to nucleotide and nucleoside analogs such as 4SU and 4TU. We were, however, able to qualitatively assess inhibition using the proxy of nascent RNA as measured by the proportion of unspliced reads in polyA+ RNA-seq datasets (Supplementary Fig. 30); we observe more than 50% reduction in unspliced reads in both α-amanitin- and triptolide-cells after 48 hours suggesting that transcription has indeed been inhibited. We also did not observe large-scale changes in the levels of individual transcripts (Supplementary Fig. 31). Finally, even at high doses, α-amanitin treatment did not detectably affect photosynthetic efficiency or cell viability relative to controls (Fig. 2C), excluding cell death as a confounding factor.

Strikingly, α-amanitin treatment resulted in a dose-dependent, progressive dinoTAD decompaction (Fig. 2D,F; Supplementary Fig. 22–25). These effects were observed in both technical and biological replicates (Supplementary Fig. 22–25). We also observed clear dose-dependent blurring of dinoTAD boundaries after triptolide treatment, though broad dinoTAD-like structures remained visible to a greater extent than in α-amanitin-treated cells (Fig. 2E-F; Supplementary Fig. 26–29).

These experiments support a transcription-induced supercoiling model for dinoTAD formation. Torque generated by active polymerases produces positive/negative supercoiling ahead of/behind the transcription bubble. This can alter the twist of the double helix or induce superhelical

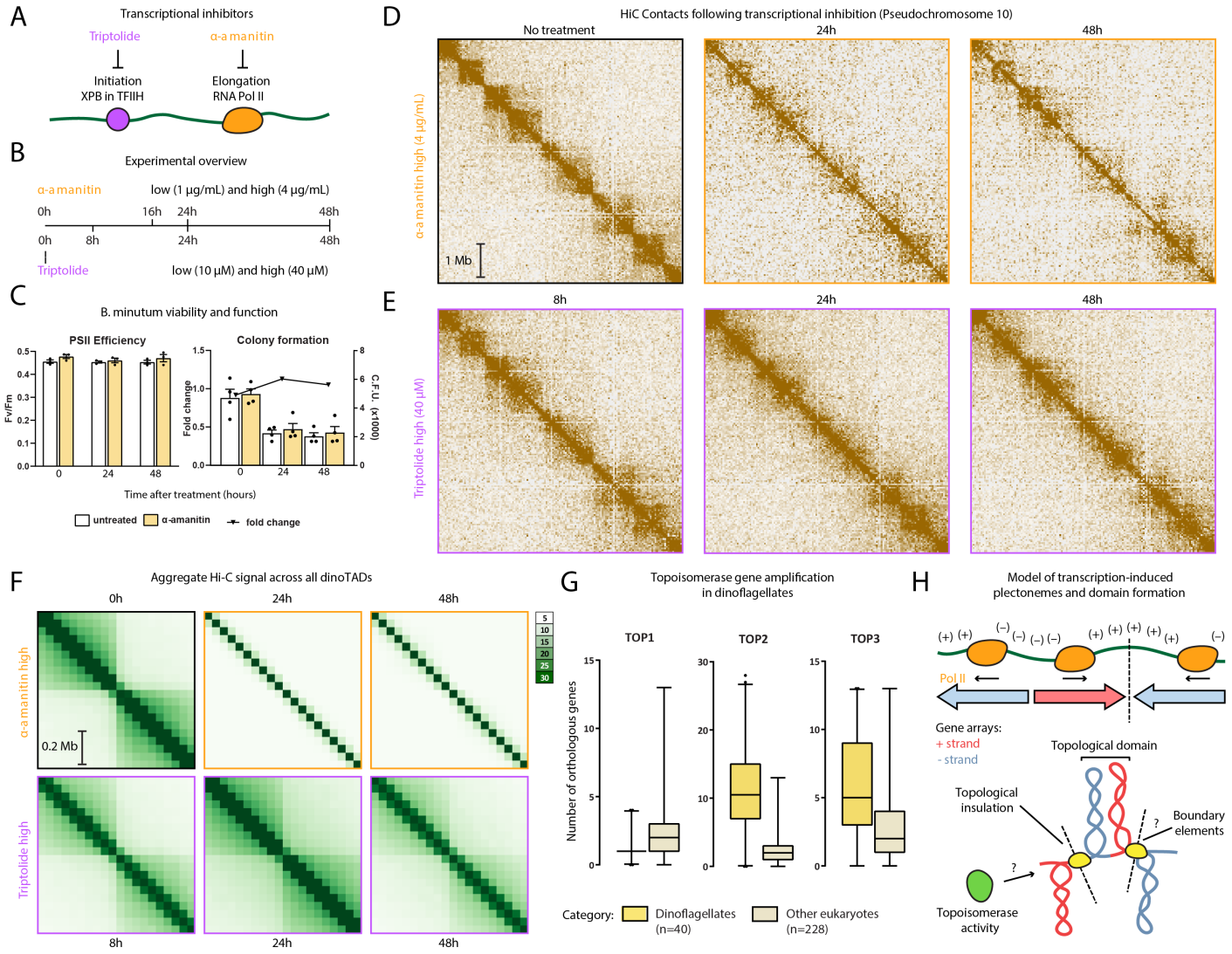

Fig. 2: Decompaction of dinoTADs upon application of transcriptional inhibitors and the transcription-induced supercoiling model for their formation. Shown is pseudochromosome 10 as in Figure 1. (A-B) Outline of transcription inhibition time course experiments. (C) Comparison of cell function, measured by PSII photosynthetic efficiency (left, $n = 3$ biological replicates for each condition), and cell viability, measured by colony formation (right; $n = 4$ biological replicates for each condition), between α-amanitin-treated and untreated cells. Treatment with α-amanitin does not affect PSII activity (Student t-test, $P = 0.75304979$ for 0h, P =0.442327976 for 24h, $P = 0.23349803$ for 48h. Error bars show mean ± SD. (D) KR-normalized Hi-C maps (50-kb resolution) show marked loss of dinoTADs after α-amanitin treatment. (E) Hi-C maps show reduction of insulation at dinoTAD boundaries after triptolide treatment. (F) Metaplots of Hi-C signal around domain boundaries (50-kb resolution). (G) Amplification of *TOP2* and *TOP3* topoisomerases in dinoflagellates (based on MMETSP [10] transcriptome assemblies). Box plots show the 25th, 50th and 75th percentiles, whiskers show the 5-95% intervals. The dinoflagellate ($n = 41$) and non-dinoflagellate ($n = 243$) species shown are the ones from Supplementary Table 2. (H) Transcription-induced supercoiling as driver of dinoflagellate chromatin folding. Transcribing polymerases introduce negative/positive DNA supercoiling behind/ahead of the transcription machinery. Interactions within supercoiled domains could explain the physical association of divergently-oriented arrays. Topological insulation could be driven by supercoiling-related effects, or by specific boundary elements.

writhe, which in turn can be accommodated through nucleosome remodeling, local alterations in DNA secondary structure, or formation of writhed structures such as plectonemes [23], from which we would expect strong Hi-C signals comprising our observed domains.

Although other topological constraints might also be involved, supercoiling-induced plectoneme formation over gene arrays is an intuitive mechanistic explanation for the

presence of dinoTADs. An examination of dinoflagellate gene repertoires also corroborates this model, revealing a striking, dinoflagellate-specific expansion of topoisomerase II- and topoisomerase III-like genes (Fig. 1D; Supplementary Fig. 18; Supplementary Table 2), further suggestive of contending with increased levels of writhed forms of helical twist.

Comparison with self-interacting domains in bacteria or *Schizosaccharomyces pombe* shows much stronger topological insulation for dinoTADs (Supplementary Fig. 15) and 16)). Remarkably, no TAD domains are observed in kinetoplastids, the other lineage with long gene arrays and no transcriptional regulation (Supplementary Fig. 17).

These differences can be rationalized by the unusual dinoflagellate properties. First, neither bacteria nor yeast possess comparably long gene arrays and transcription in those species is highly nonuniform; less transcription-induced torsional stress is therefore expected. Nucleosome loss is the second, and most salient difference. Single mammalian genes as long as dinoTADs are quite common, yet contact domains aligning with gene boundaries is not apparent in mammalian Hi-C maps, nor is it seen in kinetoplastids, which have gene arrays but also have conventional chromatin. We therefore hypothesize that plectonemic structures form due to transcription-induced supercoiling in the nucleosome-depleted genomes of dinoflagellates, while in other eukaryotes, a combination of the wrapping of DNA around nucleosomes, interactions between nucleosomes, and accumulation of DNA twist, prevent their formation (Fig. 2H).

These results generate a number of open questions. How exactly are boundaries between dinoTADs formed mechanistically? Specific boundary elements of markedly different chromatin state could exist; alternatively, these boundaries may self-organize purely through torsion-related mechanisms. The roles that dinoflagellates' divergent histone genes play is also not clear. Finally, the relationship between Hi-C features and the "toroidal chromonemas" [11] observed by electron microscopy remains unknown. Answers to these questions, together with the dissection of specific roles different topoisomerase classes, will help fully elucidate the interplay between packaging proteins, transcription-induced torsional stress, and genome folding in dinoflagellates.

These observations also identify transcription-induced torsional stress as a key direction of future studies in eukaryotes generally. The strength of dinoTADs underlines the potency of this fundamental biological process for generating topological structure. The precise manner by which torsion is accommodated as twist and writhe, as well as its consequences for regulatory protein occupancy, transcriptional activity, and other chromatin processes, such as the behavior of ATP-dependent chromatin remodelers, are exciting questions remaining to be unraveled.

Author contributions

G.K.M. performed Hi-C experiments. G.K.M and A.E.T. analyzed the data. A.E.T. and T.X. designed and carried out transcription inhibition experiments and cell viability experiments. T.X. carried out *B. minutum* culture and heat stress treatment. W.J.G., A.R.G.. A.K. and J.R.P. supervised the study. G.K.M., A.E.T. and T.X. interpreted data and wrote manuscript with input from all authors.

Acknowledgments

This work was supported by NIH grants (P50HG007735, RO1 HG008140, U19AI057266 and UM1HG009442 to W.J.G., 1UM1HG009436 to W.J.G. and A.K., 1DP2OD022870-01 and 1U01HG009431 to A.K.), the Rita Allen Foundation (to W.J.G.), the Baxter Foundation Faculty Scholar Grant, and the Human Frontiers Science Program grant RGY006S (to W.J.G). W.J.G. is a Chan Zuckerberg Biohub investigator and acknowledges grants 2017-174468 and 2018-182817 from the Chan Zuckerberg Initiative. Fellowship support provided by the Stanford School of Medicine Dean's Fellowship (G.K.M.), the Siebel Scholars, the Enhancing Diversity in Graduate Education Program and the Weiland Family Fellowship (A.E.T.). This work is also supported by NSF-IOS EDGE Award 1645164 to A.R.G. and Carnegie Venture grant 10907 (to T.X. and G.K.M.).

The authors would like to thank Andrew J. Spakowitz, Zohar Shipony, Sandy Klemm, Olga Dudchenko, Erez Lieberman Aiden, John R. Pringle, Philip Cleves, and members of the Greenleaf, Kundaje, Pringle and Grossman laboratories for helpful discussion and suggestions regarding this work.

Data Availability

Data associated with this manuscript have been submitted to GEO under accession number GSE153950

Code Availability

Custom code used to process the data is available at `https://github.com/georgimarinov/GeorgiScripts`

Competing Interests

The authors declare no competing interests.

References

1. Ramírez F, Bhardwaj V, Arrigoni L, Lam KC, Grüning BA, Villaveces J, Habermann B, Akhtar A, Manke T. 2018. High-resolution TADs reveal DNA sequences underlying genome organization in flies. *Nat Commun* **9**(1):189.

2. Szabo Q, Bantignies F, Cavalli G. 2019. Principles of genome folding into topologically associating domains. *Sci Adv* **5**(4):eaaw1668.
3. Rao SS, Huntley MH, Durand NC, Stamenova EK, Bochkov ID, Robinson JT, Sanborn AL, Machol I, Omer AD, Lander ES, Aiden EL. 2014. A 3D map of the human genome at kilobase resolution reveals principles of chromatin looping. *Cell* **159**(7):1665–1680.
4. Rowley MJ, Nichols MH, Lyu X, Ando-Kuri M, Rivera ISM, Hermetz K, Wang P, Ruan Y, Corces VG. 2017. Evolutionarily Conserved Principles Predict 3D Chromatin Organization. *Mol Cell* **67**(5):837-852.
5. Hackett JD, Anderson DM, Erdner DL, Bhattacharya D. 2004. Dinoflagellates: a remarkable evolutionary experiment. *Am J Bot* **91**:1523–1534.
6. Postberg J, Forcob S, Chang WJ, Lipps HJ. 2010. The evolutionary history of histone H3 suggests a deep eukaryotic root of chromatin modifying mechanisms. *BMC Evol Biol* **10**:259.
7. Marinov GK, Lynch M. 2015. Diversity and Divergence of Dinoflagellate Histone Proteins. *G3 (Bethesda)* **6**(2):397–422.
8. Janouškovec J, Gavelis GS, Burki F, Dinh D, Bachvaroff TR, Gornik SG, Bright KJ, Imanian B, Strom SL, Delwiche CF, Waller RF, Fensome RA, Leander BS, Rohwer FL, Saldarriaga JF. 2017. Major transitions in dinoflagellate evolution unveiled by phylotranscriptomics. *Proc Natl Acad Sci U S A* **114**(2):E171–E180.
9. Shoguchi E, Shinzato C, Kawashima T, Gyoja F, Mungpakdee S, Koyanagi R, Takeuchi T, Hisata K, Tanaka M, Fujiwara M, Hamada M, Seidi A, Fujie M, Usami T, Goto H, Yamasaki S, Arakaki N, Suzuki Y, Sugano S, Toyoda A, Kuroki Y, Fujiyama A, Medina M, Coffroth MA, Bhattacharya D, Satoh N. 2013. Draft assembly of the *Symbiodinium minutum* nuclear genome reveals dinoflagellate gene structure. *Curr Biol* **23**(15):1399–1408.
10. Keeling PJ, Burki F, Wilcox HM, Allam B, Allen EE, Amaral-Zettler LA, Armbrust EV, Archibald JM, Bharti AK, Bell CJ, Beszteri B, Bidle KD, Cameron CT, Campbell L, Caron DA, Cattolico RA, Collier JL, Coyne K, Davy SK, Deschamps P, Dyhrman ST, Edvardsen B, Gates RD, Gobler CJ, Greenwood SJ, Guida SM, Jacobi JL, Jakobsen KS, James ER, Jenkins B, John U, Johnson MD, Juhl AR, Kamp A, Katz LA, Kiene R, Kudryavtsev A, Leander BS, Lin S, Lovejoy C, Lynn D, Marchetti A, McManus G, Nedelcu AM, Menden-Deuer S, Miceli C, Mock T, Montresor M, Moran MA, Murray S, Nadathur G, Nagai S, Ngam PB, Palenik B, Pawlowski J, Petroni G, Piganeau G, Posewitz MC, Rengefors K, Romano G, Rumpho ME, Rynearson T, Schilling KB, Schroeder DC, Simpson AG, Slamovits CH, Smith DR, Smith GJ, Smith SR, Sosik HM, Stief P, Theriot E, Twary SN, Umale PE, Vaulot D, Wawrik B, Wheeler GL, Wilson WH, Xu Y, Zingone A, Worden AZ. 2014. The Marine Microbial Eukaryote Transcriptome Sequencing Project (MMETSP): illuminating the functional diversity of eukaryotic life in the oceans through transcriptome sequencing. *PLoS Biol* **12**(6):e1001889.
11. Oakley BR. Dodge JD. 1979. Evidence for a double-helically coiled toroidal chromonema in the dinoflagellate chromosome. *Chromosoma* **70**:277–291.
12. Livolant F, Bouligand, Y. 1978. New observations on the twisted arrangement of dinoflagellate chromosomes. *Chromosoma* **68**:21–44.
13. Levi-Setti R, Gavrilov KL, Rizzo PJ. 2008. Divalent cation distribution in dinoflagellate chromosomes imaged by high-resolution ion probe mass spectrometry. *Eur J Cell Biol* **87**(12):963–976.
14. Spector DL, Triemer RE. 1981. Chromosome structure and mitosis in the dinoflagellates: an ultrastructural approach to an evolutionary problem. *Biosystems* **14**(3–4):289–298.
15. Le TB, Imakaev MV, Mirny LA, Laub MT. 2013. High-resolution mapping of the spatial organization of a bacterial chromosome. *Science* **342**(6159):731–734.
16. Benedetti F, Racko D, Dorier J, Burnier Y, Stasiak A. 2017. Transcription-induced supercoiling explains formation of self-interacting chromatin domains in *S. pombe*. *Nucleic Acids Res* **45**(17):9850–9859.
17. Livolant F, Bouligand Y. 1980. Double helical arrangement of spread dinoflagellate chromosomes. *Chromosoma* **80**:97–118.
18. Wong JTY. 2019. Architectural Organization of Dinoflagellate Liquid Crystalline Chromosomes. *Microorganisms* **7**(2):27.
19. Levin RA, Beltran VH, Hill R, Kjelleberg S, McDougald D, Steinberg PD, van Oppen MJ. 2016. Sex, Scavengers, and Chaperones: Transcriptome Secrets of Divergent Symbiodinium Thermal Tolerances. *Mol Biol Evol* **33**(9):2201–2215.
20. Bensaude O. 2011. Inhibiting eukaryotic transcription: Which compound to choose? How to evaluate its activity? *Transcription* **2**(3):103–108.
21. Rizzo PJ. 1979. RNA synthesis in isolated nuclei of the dinoflagellate *Crypthecodinium cohnii*. *J Protozool* **26**(2):290–294.
22. Herzog VA, Reichholf B, Neumann T, Rescheneder P, Bhat P, Burkard TR, Wlotzka W, von Haeseler A, Zuber J, Ameres SL. 2017. Thiol-linked alkylation of RNA to assess expression dynamics. *Nat Methods* **14**(12):1198–1204.
23. Teves SS, Henikoff S. 2014. DNA torsion as a feedback mediator of transcription and chromatin dynamics. *Nucleus* **5**(3):211–218.
24. Xiang T, Hambleton EA, DeNofrio JC, Pringle JR, Grossman AR. 2013. Isolation of clonal axenic strains of the symbiotic dinoflagellate *Symbiodinium* and their growth and host specificity. *J Phycol* **49**(3):447–458.

25. Xiang T, Nelson W, Rodriguez J, Tolleter D, Grossman AR. 2015. *Symbiodinium* transcriptome and global responses of cells to immediate changes in light intensity when grown under autotrophic or mixotrophic conditions. *Plant J* **82**(1):67–80.
26. Durand NC, Shamim MS, Machol I, Rao SS, Huntley MH, Lander ES, Aiden EL. 2016. Juicer Provides a One-Click System for Analyzing Loop-Resolution Hi-C Experiments. *Cell Syst* **3**(1):95–98.
27. Dudchenko O, Batra SS, Omer AD, Nyquist SK, Hoeger M, Durand NC, Shamim MS, Machol I, Lander ES, Aiden AP, Aiden EL. 2017. De novo assembly of the *Aedes aegypti* genome using Hi-C yields chromosome-length scaffolds. *Science* **356**(6333):92–95.
28. Dobin A, Davis CA, Schlesinger F, Drenkow J, Zaleski C, Jha S, Batut P, Chaisson M, Gingeras TR. 2013. STAR: ultrafast universal RNA-seq aligner. *Bioinformatics* **29**(1):15–21.
29. Langmead B, Trapnell C, Pop M, Salzberg SL. 2009. Ultrafast and memory-efficient alignment of short DNA sequences to the human genome. *Genome Biol* **10**(3):R25.
30. Roberts A, Pachter L. 2013. Streaming fragment assignment for real-time analysis of sequencing experiments. *Nat Methods* **10**(1):71-73.
31. Love MI, Huber W, Anders S. 2014. Moderated estimation of fold change and dispersion for RNA-seq data with DESeq2. *Genome Biol* **15**(12):550.
32. Pertea M, Pertea GM, Antonescu CM, Chang TC, Mendell JT, Salzberg SL. 2015. StringTie enables improved reconstruction of a transcriptome from RNA-seq reads. *Nat Biotechnol* **33**(3):290-295.
33. Eddy SR. 2011. Accelerated Profile HMM Searches. *PLoS Comput Biol* **7**(10):e1002195.
34. Finn RD, Bateman A, Clements J, Coggill P, Eberhardt RY, Eddy SR, Heger A, Hetherington K, Holm L, Mistry J, Sonnhammer EL, Tate J, Punta M. 2014. Pfam: the protein families database. *Nucleic Acids Res* **42**(Database issue):D222–230.
35. Knight P, Ruiz D. 2013. A fast algorithm for matrix balancing. *IMA J Num Anal* **33**(3):1029–1047.
36. Hou Y, Ji N, Zhang H, Shi X, Han H, Lin S. 2019. Genome size-dependent pcna gene copy number in dinoflagellates and molecular evidence of retroposition as a major evolutionary mechanism. *J Phycol* **55**(1):37–46.

Methods

Except where otherwise stated, computational analyses were carried out using custom-written Python scripts.

B. minutum cell culture

The clonal axenic *B. minutum* strain SSB01 was used in all experiments. Stock cultures were grown as previously described[24,25] in Daigo's IMK medium for marine microalgae (Wako Pure Chemicals) supplemented with casein hydrolysate (IMK+Cas) at 27 °C at a light intensity of 10 μmol photons m^{-2} s^{-1} from Philips ALTO II 25-W bulbs on a 12-h-light:12-h-dark cycle. The medium was prepared in artificial seawater (ASW).

Transcription inhibition experiments

For α-amanitin treatment, *B. minutum* cells at a density of $\sim$1 $\times 10^6$ cells/ml were treated with α-amanitin (Sigma-Aldrich, Cat # A2263) at concentrations of 1 μg/mL ("normal" dose) and 4 μg/ml ("high") dose.

Samples were harvested at 0, 24, and 48 hours after treatment.

For triptolide treatment, *B. minutum* cells at a density of $\sim$1 $\times 10^6$ cells/ml were treated with triptolide (Sigma-Aldrich, Cat # T3652) at concentrations of 10 μM ("normal" dose) and 40 μM ("high") dose.

Samples were harvested at 0, 8, 24 and 48 hours after treatment.

Cell viability measurements

Photosynthetic activity

Maximum quantum yields of photosystem II, $Fv/Fm = (Fm - F0)/Fm$ was used to indicate photosynthetic function. *B. minutum* cultures (approximately 10^6 cells/ml) were collected and dark adapted for 5 min, and Fv/Fm was determined using a Dual Pam-100 fluorometer (Heinz Walz).

Colony formation assay

Fresh SSB01 cells were sampled at 0, 24 and 48 hours after the treatment of transcription inhibitor α-amanitin. For each condition, cell suspensions were diluted 1:5 and 1:10 before plating 1 μl of each dilution on marine broth (BD) agar plates. Plates were incubated at 27 °C at a light intensity of 10 μmol photons m^2 s^1. Cell numbers on each plate were counted after three weeks.

Hi-C experiments

The in situ Hi-C procedure used to map 3D genomic interactions in *B. minutum* was adapted from previous studies[3] as follows:

B. minutum SSBO1 cells were first crosslinked using 37% formaldehyde (Sigma) at a final concentration of 1% for 15 minutes at room temperature. Formaldehyde was then quenched using 2.5 M Glycine at a final concentration of 0.25 M. Cells were subsequently centrifuged at 2,000 *g* for 5 minutes, washed once in 1× PBS, and stored at -80 °C.

Cell lysis was initiated by incubation with 250 μl of cold Hi-C Lysis Buffer (10 mM Tris-HCl pH 8.0, 10 mM NaCl, 0.2% Igepal CA630) on ice for 15 minutes, followed by centrifugation at 2,500 *g* for 5 minutes, a wash with 500 μl of cold Hi-C Lysis Buffer, and centrifugation at 2,500 *g* for 5 minutes. The pellet was the resuspended in 50 μl of 0.5% SDS and incubated at 62 °C for 10 minutes (except for the "no-denaturation sample, for which the pellet was resuspended in 50 μl H_2O). SDS was quenched by adding 145 μl of H_2O and 25 μl of 10% Triton X-100 and incubating at 37 °C for 15 minutes.

Restriction digestion was carried out by adding 25 μl of 10× NEBuffer 2 and 100 U of the MboI restriction enzyme (NEB, R0147) and incubating for $\geq$2 hours at 37 °C in a Thermomixer at 900 rpm. The reaction was then incubated at 62 °C for 20 minutes in order to inactivate the restriction enzyme.

Fragment ends were filled in by adding 37.5 μl of 0.4 mM biotin-14-dATP (ThermoFisher Scientific, # 19524-016), 1.5 μl each of 10 mM dCTP, dGTP and dTTP, and 8 μl of 5U/μl DNA Polymerase I Large (Klenow) Fragment (NEB M0210). The reaction was the incubated at 37 °C in a Thermomixer at 900 rpm for 45 minutes.

Fragment end ligation was carried out by adding 663 μl H_2O, 120 μl 10× NEB T4 DNA ligase buffer (NEB B0202), 100 μl of 10% Triton X-100, 12 μl of 10 mg/ml Bovine Serum Albumin (100× BSA, NEB), 5 μl of 400 U/μl T4 DNA Ligase (NEB M0202), and incubating at room temperature for $\geq$4 hours with rotation.

Nuclei were then pelleted by centrifugation at 3,500 *g* for 5 minutes; the pellet was resuspended in 200 μl ChIP Elution Buffer (1% SDS, 0.1 M $NaHCO_3$), Proteinase K was added, and incubated at 65 °C overnight to reverse crosslinks.

After addition of 600 μl 1×TE buffer, DNA was sonicated using a Qsonica S-4000 with a 1/16" tip for 3 minutes, with 10 second pulses at intensity 3.5, and 20 seconds rest between pulses. DNA was then purified using the MinElute PCR Purification Kit (Qiagen #28006), with elution in a total volume of 300 μl 1× EB buffer.

For streptavidin pulldown of biotin-labeled DNA, 150 μl of 10 mg/ml Dynabeads MyOne Streptavidin T1 beads (Life Technologies, 65602) were separated on a magnetic stand, then washed with 400 μl of 1× TWB (Tween Washing Buffer; 5 mM Tris-HCl pH 7.5; 0.5 mM EDTA; 1 M NaCl; 0.05% Tween 20). The beads were resuspended in 300 μl of 2× Binding Buffer (10 mM Tris-HCl pH 7.5, 1 mM EDTA; 2 M NaCl), the sonicated DNA was added, and

the beads were incubated for ≥15 minutes at room temperature on a rotator. After separation on a magnetic stand, the beads were washed with 600 μl of 1× TWB, and heated at 55 °C in a Thermomixer with shaking for 2 minutes. After removal of the supernatant on a magnetic stand, the TWB wash and 55 °C incubation were repeated.

Final libraries were prepared on beads using the NEBNext Ultra II DNA Library Prep Kit (NEB, #E7645) as follows. End repair was carried out by resuspending beads in 50 μl 1× EB buffer, and adding 3 μl NEB Ultra End Repair Enzyme and 7 μl NEB Ultra End Repair Enzyme, followed by incubation at 20 °C for 30 minutes and then at 65 °C for 30 minutes.

Adapters were ligated to DNA fragments by adding 30 μl Blunt Ligation mix, 1 μl Ligation Enhancer and 2.5 μl NEB Adapter, incubating at 20 °C for 20 minutes, adding 3 μl USER enzyme, and incubating at 37 °C for 15 minutes.

Beads were then separated on a magnetic stand, and washed with 600 μl TWB for 2 minutes at 55 °C, 1000 rpm in a Thermomixer. After separation on a magnetic stand, beads were washed in 100 μl 0.1 × TE buffer, then resuspended in 16 μl 0.1 × TE buffer, and heated at 98 °C for 10 minutes.

For PCR, 5 μl of each of the i5 and i7 NEB Next sequencing adapters were added together with 25 μl 2× NEB Ultra PCR Mater Mix. PCR was carried out with a 98 °C incubation for 30 seconds and 12 cycles of 98 °C for 10 seconds, 65 °C for 30 seconds, and 72 °C for 1 minute, followed by incubation at 72 °C for 5 minutes.

Beads were separated on a magnetic stand, and the supernatant was cleaned up using 1× AMPure XP beads.

Libraries were sequenced in a paired-end format on a Illumina NextSeq instrument using NextSeq 500/550 high output kits (either 2×75 or 2×36 cycles).

Hi-C data processing and assembly scaffolding

As an initial step, Hi-C sequencing reads from all libraries were trimmed of adapter sequences, pooled together, and processed against the previously published *B. minutum* assembly[9] using the Juicer pipeline[26] for analyzing Hi-C datasets (version 1.8.9 of Juicer Tools).

The resulting Hi-C matrices were then used as input to the 3D DNA pipeline[27] for automated scaffolding with the following parameters: `--editor-coarse-resolution 5000 --editor-coarse-region 5000 --polisher-input-size 100000 --polisher-coarse-resolution 1000 --polisher-coarse-region 300000 --splitter-input-size 100000 --splitter-coarse-resolution 5000 --splitter-coarse-region 300000 --sort-output --build-gapped-map -r 10 -i 5000`.

Manual correction of obvious assembly and scaffolding errors was then carried out using Juicebox[26].

After finalizing the scaffolding, Hi-C reads were reprocessed against the new assembly using the Juicer pipeline. This was done individually for each library as well as together for the pooled set of reads.

Data were extracted from the final read matrices using the Juicer suite of tools for Hi-C data analysis.

Identification of Hi-C domains

Hi-C matrices were first converted to *cool* format using HiCExplorer[1] "`hicConvertFormat`" with parameters `--inputFormat hic --outputFormat h5` and default resolutions. Subsequent HiCExplorer commands were carried out at 10-kb, 25-kb, and 50-kb resolutions; the 50-kb domains were used for subsequent analysis as they matched visually apparent domain boundaries best. Matrices were normalized using "`hicNormalize`" with parameter `--normalize smallest`, and corrected using "`hicCorrectMatrix correct`" with parameters `--correctionMethod KR`. Hi-C domains were computationally identified using the "`hicFindTADs`" from HiCExplorer with parameter `--correctForMultipleTesting fdr`. The domains derived from the 50-kb resolution analysis were used for subsequent analyses.

RNA-seq experiments

Total RNA was isolated following previously described protocols[25].

RNA-seq libraries were generated after selection of polyadenylated RNA using the Nebnext Poly(A) mRNA Magnetic Isolation Module (NEB E7490) and using the NEBNext Ultra II Directional RNA Library Prep (NEB E7765), following manufacturer's instructions.

RNA-seq data analysis

For the analysis of unspliced transcripts, RNA-seq reads were aligned against the original *B. minitum* assembly and annotation using the STAR aligner[28] (version 2.5.3a) with the following settings: `--limitSjdbInsertNsj 10000000 --outFilterMultimapNmax 50 --outFilterMismatchNmax 999 --outFilterMismatchNoverReadLmax 0.04 --alignIntronMin 10 --alignIntronMax 1000000 --alignMatesGapMax 1000000 --alignSJoverhangMin 8 --alignSJDBoverhangMin 1 --sjdbScore 1 --twopassMode Basic --twopass1readsN -1`. The fraction of intronic reads was estimated from the resulting BAM files.

For the purpose of differential expression analysis, reads were aligned against the transcriptome space using Bowtie[29] (version 1.0.1) with the following settings: `-e 200 -a` and quantified using eXpress[30] (version 1.5.1). The resulting effective counts were used as input to DESeq2[31] for differential expression analysis. An adjusted P-value threshold of 0.05 was used to derive lists of significantly differential genes.

External RNA-seq datasets

Approximately 5×10^7 cells were collected by centrifugation at 100 g for 5 minutes at room temperature. Total RNA was extracted and libraries were constructed for RNA-Seq using the TruSeq RNA Library Prep Kit V2 (Illumina, San Diego, CA, USA) according to the manufacturer protocol. All of the raw sequencing reads are available at Sequence Read Archive (SRA) with accession number SRX7258938.

External RNA-seq data analysis

RNA-seq reads were aligned against the corresponding assemblies using the STAR aligner[28] (version 2.5.3a) with the following settings: `--limitSjdbInsertNsj 10000000 --outFilterMultimapNmax 50 --outFilterMismatchNmax 999 --outFilterMismatchNoverReadLmax 0.04 --alignIntronMin 10 --alignIntronMax 1000000 --alignMatesGapMax 1000000 --alignSJoverhangMin 8 --alignSJDBoverhangMin 1 --sjdbScore 1 --twopassMode Basic --twopass1readsN -1`. As available RNA-seq datasets for *B. minutum* are not strand-specific, the strand orientation of the transcriptome was visualized as follows. Aligned reads were first *de novo* assembled into transcripts and quantified at the transcript level using Stringtie[32] (version 1.3.3.b); the orientation of splice junctions serves as a reliable guide for the directionality of these transcripts. Open reading frames (ORFs) were identified for each transcript, and transcripts with ORFs shorter than 60 amino acids were filtered out of the transcript set. Strand-specific genomic tracks were then generated by assigning to each basepair covered by at least one exon in that set the sum of the TPM (Transcript Per Million transcripts) values of all transcripts it is included in.

External Hi-C datasets

Hi-C datasets for *Trypanosoma brucei* were obtained from GEO accession GSE118764.

Hi-C datasets for *Schizosaccharomyces pombe* were obtained from GEO accession GSE57316.

Hi-C datasets for *Caulobacter vibrioides* CB15 were obtained from GEO accession GSE45966.

Sequence Analysis

Topoisomerase and other replication-related proteins were identified in annotated MMETSP transcriptome assemblies using HMMER3.0[33] and the Pfam 27.0 protein domain database[34] as previously described[7].

Supplementary Materials

Supplementary Tables

Supplementary Table 1: Summary of Hi-C datasets used in this studyNote that the L142 was not aligned independently against the scaffolded assembly.

Hi-C library	Number raw read pairs	Number Hi-C contacts	Inter-chromosomal	Intra-chromosomal	Short Range (<20Kb)	Long Range (>20Kb)
L142-SSBO1-HIC	534,609,924	220,908,462	n/a	n/a	n/a	n/a
L533-SSBO1_27C_Hi-C	556,089,015	151,618,419	86,874,088	64,714,851	15,980,982	48,733,566
L534-SSBO1_34C_Hi-C	531,461,453	165,231,965	105,854,838	59,340,858	15,152,077	44,188,629
L1240-SSBO1-α_amanitin-0h-Hi-C	111,333,226	34,384,671	17,570,560	16,814,111	11,264,242	5,549,754
L1241-SSB01-α_amanitin-16h-Hi-C-rep1	60,696,609	24,238,281	16,530,785	7,707,496	1,948,364	5,759,040
L1242-SSB01-α_amanitin-16h-Hi-C-rep2	67,376,168	25,551,603	16,785,702	8,765,901	2,733,314	6,032,518
L1243-SSB01-α_amanitin-24h-Hi-C-rep1	81,532,584	29,748,439	17,594,153	12,154,286	5,518,236	6,635,937
L1244-SSB01-α_amanitin-24h-Hi-C-rep2	106,381,220	28,845,306	13,249,756	15,595,550	10,678,732	4,916,732
L1245-SSB01-α_amanitin-48h-Hi-C-rep1	90,180,763	27,045,343	14,627,900	12,417,443	7,996,822	4,420,494
L1246-SSB01-α_amanitin-48h-Hi-C-rep2	78,982,528	22,153,117	10,227,616	11,925,501	9,688,693	2,236,727
L1247-SSB01-α_amanitin_high-48h-Hi-C	110,015,013	28,138,017	12,521,207	15,616,810	13,323,212	2,293,491
L1332-SSB01-α_amanitin-0h-Hi-C-technical_rep	117,543,007	34,089,285	8,856,415	9,967,696	6,932,955	3,034,688
L1332-SSB01-α_amanitin-0h-Hi-C-technical_rep (deeply sequenced)	549,347,830	117,521,684	43,073,422	74,448,262	59,815,340	14,617,472
L1333-SSB01-α_amanitin-48h-Hi-C-rep1-technical_rep	117,821,773	23,654,760	9,625,400	10,156,023	8,219,059	1,936,888
L1334-SSB01-α_amanitin_high-48h-Hi-C-technical_rep	95,662,202	23,944,231	7,954,448	7,390,838	6,704,651	686,125
L1334-SSB01-α_amanitin_high-48h-Hi-C-technical_rep (deeply sequenced)	473,889,681	121,126,963	42,613,255	78,513,708	75,375,032	3,118,515
L1336-SSB01-α_amanitin_high-24h-Hi-C-second_time_course	58,747,402	15,663,160	7,063,048	8,600,112	7,507,098	1,092,920
L1337-SSB01-α_amanitin_high-48h-Hi-C-second_time_course	83,691,617	14,523,464	4,509,911	7,483,408	6,557,471	925,885
L1344-SSB01-α_amanitin/triptolide_0h_NT-Hi-C	79,383,186	23,592,335	8,705,306	5,552,923	3,332,771	2,220,106
L1346-SSB01-triptolide_8h_normal_dose-Hi-C	81,731,190	22,700,096	9,664,851	6,591,405	4,367,366	2,223,978
L1347-SSB01-triptolide_8h_high_dose-Hi-C	112,753,865	28,552,855	12,538,332	7,793,297	5,328,647	2,464,576
L1348-SSB01-Triptolide_24h NT-Hi-C	52,148,987	15,674,551	9,064,518	6,610,033	4,572,399	2,037,564
L1349-SSB01-triptolide_24h_normal_dose-Hi-C	132,715,807	36,745,591	14,682,269	9,235,388	5,978,780	3,256,547
L1350-SSB01-triptolide_24h_high_dose-Hi-C	98,429,444	32,121,298	17,352,686	7,050,890	3,608,073	3,442,753
L1351-SSB01-Triptolide_48h NT-Hi-C	96,846,551	28,296,251	15,850,741	12,445,510	8,950,541	3,494,849
L1352-SSB01-triptolide_48h_normal_dose-Hi-C	85,347,611	25,051,605	10,201,062	8,150,528	5,678,662	2,471,791
L1353-SSB01-triptolide_48h_high_dose-Hi-C	99,978,207	26,572,806	10,201,062	8,150,528	5,678,662	2,471,791
L1859-SSB01-no_denaturation_Hi-C	66,901,271	20,405,394	11,777,718	8,627,676	3,085,753	5,541,871
L1860-SSB01-NT_third_time_course_0h_Hi-C-rep1	63,376,846	23,998,854	14,148,277	9,850,577	4,476,912	5,373,576
L1861-SSB01-NT_third_time_course_48h_Hi-C-rep1	50,110,006	20,240,831	13,072,004	7,168,827	2,969,228	4,199,554
L1862-SSB01-α-amanitin_third_time_course_48h_Hi-C-rep1	34,285,113	13,933,089	9,590,066	4,343,023	1,840,009	2,502,993
L1863-SSB01-Triptolide_third_time_course_48h_Hi-C-rep1	51,692,203	20,258,253	14,483,933	5,774,320	2,425,431	3,348,867
L1864-SSB01-NT_third_time_course_96h_washout_Hi-C-rep1	69,331,722	26,471,641	12,353,321	14,118,320	10,798,300	3,319,746
L1865-SSB01-α-amanitin_third_time_course_96h_washout_Hi-C-rep1	45,055,806	18,126,550	11,283,311	6,843,239	3,809,588	3,033,600
L1866-SSB01-Triptolide_third_time_course_96h_washout_Hi-C-rep1	54,731,637	22,146,724	14,960,287	7,186,437	3,349,384	3,837,015

Supplementary Table 2: Inventory of topoisomerases and some other proteins involved in DNA replication in dinoflagellates and other eukaryotes as annotated by transcriptome assemblies in the MMETSP databses

clade	species	TOP1	TOP2	TOP3	MCM	PCNA	RPA1	RPA2	RPA3	RFC1
Amoebozoa	*Stereomyxa ramosa* Chinc5	1	2	2	6	2	3	0	2	1
Amoebozoa	*Vexillifera* sp. DIVA3 564 2	1	2	2	7	1	2	0	0	1
Apicomplexa	*Lankesteria abbottii* Grappler Inlet BC	1	1	0	12	5	1	0	0	1
Bicosoecid	Bicosoecid sp ms1	1	0	0	3	1	1	1	1	0
Bicosoecid	*Cafeteria roenbergensis* E4 10	1	0	2	6	1	0	0	1	0
Bicosoecid	*Cafeteria* sp. Caron Lab Isolate	1	1	4	15	1	1	0	1	1
Bolidophyte	*Bolidomonas pacifica* CCMP 1866	2	5	7	8	1	1	0	0	1
Chlorarachniophyte	*Bigelowiella natans* CCMP1258.1	1	1	9	3	1	4	1	0	0
Chlorarachniophyte	*Bigelowiella natans* CCMP1259	1	1	6	7	1	4	1	0	1
Chlorarachniophyte	*Bigelowiella natans* CCMP 2755	0	0	4	5	1	4	1	0	1
Chlorarachniophyte	*Bigelowiella natans* CCMP623	1	3	7	9	1	2	1	0	1
Chlorarachniophyte	*Chlorarachnion reptans* CCCM449	2	4	8	11	2	3	1	0	1
Chlorarachniophyte	*Lotharella amoebiformis* CCMP2058	2	6	5	10	1	4	1	0	1
Chlorarachniophyte	*Lotharella globosa* CCCM811	1	2	1	0	1	1	1	1	1
Chlorarachniophyte	*Lotharella oceanica* CCMP622	1	0	0	1	1	2	1	1	1
Chlorarachniophyte	*Norrisiella sphaerica* BC52	1	0	3	0	1	2	1	1	0
Chlorarachniophyte	*Partenskyella glossopodia* RCC365	1	2	1	7	1	3	1	2	1
Chlorophyte	*Bathycoccus prasinos* CCMP1898	1	2	3	9	1	2	0	0	0
Chlorophyte	*Bathycoccus prasinos* RCC716	1	2	3	7	1	3	0	0	1
Chlorophyte	*Chlamydomonas* cf sp CCMP681	1	0	0	5	2	1	0	0	1
Chlorophyte	*Crustomastix stigmata* CCMP3273	1	2	4	10	1	1	1	0	1
Chlorophyte	*Cyanoptyche gloeocystis* SAG4.97	1	0	0	4	1	1	1	0	0
Chlorophyte	*Dolichomastix tenuilepis* CCMP3274	1	1	3	1	2	1	0	1	1
Chlorophyte	*Dunaliella tertiolecta* CCMP1320	1	2	3	10	1	2	0	1	1
Chlorophyte	*Mantoniella antarctica* SL 175	1	8	4	13	1	2	2	1	1
Chlorophyte	*Mantoniella* sp CCMP1436	1	2	1	2	1	1	1	1	1
Chlorophyte	*Micromonas* sp CCMP2099	1	2	2	9	1	2	0	1	1
Chlorophyte	*Micromonas* sp NEPCC29	1	2	3	7	1	2	0	1	1
Chlorophyte	*Micromonas* sp RCC472	1	2	2	7	1	2	1	0	1
Chlorophyte	*Nephroselmis pyriformis* CCMP717	1	4	8	10	1	2	0	1	1
Chlorophyte	*Picochlorum oklahomensis* CCMP2329	1	2	2	6	2	2	1	0	1
Chlorophyte	*Picochlorum* sp. RCC944	1	1	2	6	1	2	0	2	1
Chlorophyte	*Picocystis salinarum* CCMP1897	1	2	1	8	2	2	1	2	1
Chlorophyte	*Polytomella parva* SAG 63 3	1	5	3	18	2	3	0	0	1
Chlorophyte	*Prasinoderma coloniale* CCMP1413	1	2	0	2	1	1	0	0	0
Chlorophyte	*Prasinoderma singularis* RCC927	1	1	1	7	1	1	0	1	1
Chlorophyte	*Pterosperma* sp. CCMP1384	1	0	0	3	1	1	1	1	1
Chlorophyte	*Pycnococcus provasolii* RCC2336	1	1	0	9	1	1	0	0	1
Chlorophyte	*Pycnococcus provasolii* RCC931	1	0	0	7	1	1	0	0	1
Chlorophyte	*Pyramimonas parkeae* CCMP726	1	0	4	7	1	2	1	1	1
Chlorophyte	*Stichococcus* sp RCC1054	1	1	1	8	1	1	0	0	1
Chlorophyte	*Tetraselmis chuii* PLY429	2	0	0	0	0	2	0	1	2
Chlorophyte	*Tetraselmis striata* LANL1001	1	4	4	11	1	2	0	1	1
Choanoflagellata	*Acanthoeca* like sp 10tr	1	3	4	10	1	1	0	1	1
Chromerida	*Chromera velia* CCMP2878	1	1	3	10	2	2	0	0	1
Chromerida	*Vitrella brassicaformis* CCMP3346	1	1	2	9	2	1	0	0	1
Chrysophyte	*Chromulina nebulosa* UTEXLB2642	1	1	1	2	1	1	0	0	1
Chrysophyte	*Dinobryon* sp UTEXLB2267	1	3	0	8	1	1	0	0	1
Chrysophyte	*Mallomonas* Sp CCMP3275	1	2	1	9	1	1	0	1	1
Chrysophyte	*Ochromonas* sp CCMP1393	1	2	2	7	1	1	0	0	1
Chrysophyte	*Paraphysomonas bandaiensis* Caron Lab Isolate	1	2	3	9	2	1	1	1	1
Chrysophyte	*Paraphysomonas imperforata* PA2	0	1	3	6	1	1	1	1	1
Chrysophyte	*Pelagococcus subviridis* CCMP1429	1	1	2	11	1	0	0	0	1
Chrysophyte	*Spumella elongata* CCAP 955 1	1	1	3	10	4	3	0	1	1
Ciliate	*Aristerostoma* sp. ATCC 50986	2	1	1	0	2	1	0	0	2
Ciliate	*Blepharisma japonicum* Stock R1072	0	0	0	7	4	1	0	0	0

Continued on next page

Supplementary Table 2 – *Continued from previous page*

clade	species	TOP1	TOP2	TOP3	MCM	PCNA	RPA1	RPA2	RPA3	RFC1
Ciliate	*Climacostomum virens* Stock W 24	1	2	2	9	3	1	0	0	3
Ciliate	*Condylostoma magnum* COL2	0	0	0	2	0	0	0	0	0
Ciliate	*Euplotes focardii* TN1	1	0	0	5	2	1	0	2	0
Ciliate	*Euplotes harpa* FSP1.4	2	0	5	3	1	0	0	1	0
Ciliate	*Fabrea salina* Unknown	1	1	3	7	2	3	0	0	2
Ciliate	*Favella taraikaensis* FeNarragansettBay	0	1	2	7	3	0	0	0	0
Ciliate	*Litonotus pictus* P1	1	1	2	0	0	0	0	0	0
Ciliate	*Mesodinium pulex* SPMC105	2	13	2	16	9	4	0	0	6
Ciliate	*Myrionecta rubra* CCMP2563	0	1	4	11	1	1	0	1	0
Ciliate	*Platyophrya macrostoma* WH	4	4	4	23	4	6	0	0	3
Ciliate	*Protocruzia adherens* Boccale	3	1	0	9	3	3	0	0	1
Ciliate	*Pseudokeronopsis* sp. OXSARD2	1	1	1	6	1	0	0	1	1
Ciliate	*Strombidinopsis acuminatum* SPMC142	2	6	0	32	10	5	0	0	0
Ciliate	*Strombidinopsis* sp. SopsisLIS2011	1	0	0	8	3	2	0	0	0
Ciliate	*Strombidium* inclinatum S3	1	1	2	8	1	1	0	0	1
Ciliate	*Strombidium rassoulzadegani* ras09	1	0	1	6	1	1	0	1	0
Ciliate	*Tiarina fusus* LIS	1	7	3	16	3	4	2	1	1
Cryptophyte	*Chroomonas mesostigmatica* cf CCMP1168	1	5	4	8	1	2	2	0	1
Cryptophyte	*Cryptomonas curvata* CCAP979 52	2	0	2	0	1	1	0	1	0
Cryptophyte	*Cryptomonas paramecium* CCAP977 2a	3	2	2	5	1	1	0	0	1
Cryptophyte	*Geminigera cryophila* CCMP2564	2	1	5	11	1	2	0	1	2
Cryptophyte	*Geminigera* sp. Caron Lab Isolate	1	3	5	18	1	5	0	1	1
Cryptophyte	*Goniomonas pacifica* CCMP1869	8	4	4	12	1	5	1	3	7
Cryptophyte	*Guillardia theta* CCMP 2712	1	0	2	3	1	1	0	1	0
Cryptophyte	*Hemiselmis andersenii* CCMP644	1	2	5	12	1	2	0	1	1
Cryptophyte	*Hemiselmis rufescens* PCC563	1	0	3	7	1	1	1	1	1
Cryptophyte	*Hemiselmis tepida* CCMP443	3	2	0	3	1	1	1	1	1
Cryptophyte	*Hemiselmis viresens* PCC157	1	0	0	7	1	1	0	1	0
Cryptophyte	*Palpitomonas bilix* NIES 2562	0	1	2	13	4	3	0	1	3
Cryptophyte	*Proteomonas sulcata* CCMP704	0	1	0	3	1	1	0	0	1
Cryptophyte	*Rhodomonas lens* RHODO	2	3	2	2	2	2	0	1	0
Cryptophyte	*Rhodomonas* sp. CCMP768	1	0	1	0	1	1	0	0	0
Diatome	*Amphiprora* sp.	1	4	3	9	1	1	0	0	1
Diatome	*Amphora coffeaeformis* CCMP127	1	1	0	4	1	1	0	0	0
Diatome	*Asterionellopsis glacialis* CCMP134	1	7	1	10	1	1	0	0	1
Diatome	*Astrosyne radiata* 13vi08 1A	1	8	3	6	3	2	0	0	1
Diatome	*Attheya septentrionalis* CCMP2084	1	2	0	9	1	1	0	0	1
Diatome	*Aulacoseira subarctica* CCAP 1002 5	1	2	3	8	2	1	0	0	1
Diatome	*Chaetoceros affinis* CCMP159	1	3	1	8	1	1	0	0	1
Diatome	*Chaetoceros curvisetus*	1	4	4	6	1	3	0	0	1
Diatome	*Chaetoceros debilis* MM31A_1	1	3	1	12	1	1	0	0	1
Diatome	*Chaetoceros neogracile* CCMP1317	1	9	3	10	1	1	0	1	1
Diatome	*Coscinodiscus wailesii* CCMP2513	1	3	6	10	1	1	0	1	1
Diatome	*Craspedostauros australis* CCMP3328	1	0	0	4	0	1	0	0	0
Diatome	*Cyclophora tenuis* ECT3854	1	1	0	3	1	1	0	0	0
Diatome	*Cyclotella meneghiniana* CCMP 338	1	4	3	8	1	1	0	0	1
Diatome	*Cylindrotheca closterium* KMMCC:B 181	3	7	3	14	1	2	0	0	1
Diatome	*Dactyliosolen fragilissimus* Unknown	1	3	3	8	1	1	0	1	1
Diatome	*Ditylum brightwellii* GSO103	1	4	3	11	1	1	0	1	1
Diatome	*Ditylum brightwellii* GSO104	1	4	5	10	1	1	0	1	1
Diatome	*Ditylum brightwellii* GSO105	1	2	3	11	2	1	0	1	1
Diatome	*Entomoneis* sp. CCMP2396	0	1	0	0	1	1	0	0	0
Diatome	*Eucampia antarctica* CCMP1452	1	3	0	5	1	1	1	1	1
Diatome	*Extubocellulus spinifer* CCMP396	1	4	10	13	2	5	3	1	2
Diatome	*Fragilariopsis kerguelensis* L2_C3	1	3	3	11	1	1	2	0	1
Diatome	*Fragilariopsis kerguelensis* L26_C5	1	3	5	22	1	1	3	0	1
Diatome	*Grammatophora oceanica* CCMP 410	1	1	3	5	1	1	0	0	1
Diatome	*Helicotheca tamensis* CCMP826	0	1	0	1	1	1	0	1	0
Diatome	*Leptocylindrus danicus* var. apora B651	3	5	3	0	3	2	0	1	1

Continued on next page

Supplementary Table 2 – *Continued from previous page*

clade	species	TOP1	TOP2	TOP3	MCM	PCNA	RPA1	RPA2	RPA3	RFC1
Diatome	*Leptocylindrus danicus* var. danicus B650	3	11	3	19	1	1	0	1	2
Diatome	*Licmophora paradoxa* CCMP2313	1	1	3	7	1	2	0	0	1
Diatome	*Minutocellus polymorphus* CCMP3303	0	0	0	3	1	1	1	1	0
Diatome	*Minutocellus polymorphus* NH13	2	8	7	21	1	0	1	0	3
Diatome	*Minutocellus polymorphus* RCC2270	1	2	1	7	1	1	1	1	1
Diatome	*Nitzschia punctata* CCMP561	1	2	2	9	1	1	1	1	1
Diatome	*Odontella aurita* isolate 1302 5	1	3	7	11	2	2	1	1	1
Diatome	*Odontella sinensis* Grunow 1884	1	3	0	2	1	1	1	1	1
Diatome	*Proboscia alata* PI_D3	1	7	2	21	1	1	2	0	1
Diatome	*Pseudo-nitzschia australis* 10249_10_AB	1	3	4	8	1	1	1	0	1
Diatome	*Pseudo-nitzschia fradulenta* WWA7	2	11	6	24	4	5	0	0	3
Diatome	*Rhizosolenia setigera* CCMP 1694	1	7	4	18	1	2	0	0	2
Diatome	*Skeletonema dohrnii* SkelB	1	2	0	14	1	1	2	1	1
Diatome	*Skeletonema marinoi* SkelA	1	1	2	7	1	1	2	0	1
Diatome	*Skeletonema menzelii* CCMP793	1	4	4	8	1	1	2	0	1
Diatome	*Stauroneis constricta* CCMP1120	1	0	1	1	1	1	1	0	0
Diatome	*Staurosira complex* sp. CCMP2646	1	3	4	8	1	1	0	1	1
Diatome	*Stephanopyxis turris* CCMP 815	2	0	1	7	3	2	0	1	1
Diatome	*Striatella unipunctata* CCMP2910	4	2	1	6	3	0	1	0	2
Diatome	*Synedropsis recta* cf CCMP1620	1	2	0	1	1	1	1	1	0
Diatome	*Thalassionema frauenfeldii* CCMP 1798	1	5	7	15	1	3	1	1	2
Diatome	*Thalassionema nitzschioides* L26_B	1	3	4	8	1	1	1	1	1
Diatome	*Thalassiosira antarctica* CCMP982	1	4	2	12	1	1	3	1	1
Diatome	*Thalassiosira gravida* GMp14c1	1	1	3	13	1	1	2	1	1
Diatome	*Thalassiosira miniscula* CCMP1093	1	13	6	10	1	1	2	1	1
Diatome	*Thalassiosira oceanica* CCMP1005	1	10	1	10	1	1	0	0	1
Diatome	*Thalassiosira rotula* CCMP3096	1	5	3	11	1	1	2	1	1
Diatome	*Thalassiosira rotula* GSO102	1	3	2	11	1	1	1	1	1
Diatome	*Thalassiosira weissflogii* CCMP1010	1	4	1	9	1	0	1	0	1
Diatome	*Thalassiosira weissflogii* CCMP1336	1	4	1	8	1	0	1	0	1
Diatome	*Thalassiothrix antarctica* L6_D1	1	2	4	6	1	1	0	1	1
Diatome	*Triceratium dubium* CCMP147	0	1	1	1	1	0	1	1	0
Dinoflagellata	*Alexandrium temarense* CCMP1771	3	18	12	45	18	10	3	4	2
Dinoflagellata	*Amphidinium carterae* CCMP1314	2	5	5	8	2	4	0	0	3
Dinoflagellata	*Azadinium spinosum* 3D9	1	12	13	35	11	6	0	0	3
Dinoflagellata	*Brandtodinium nutriculum* RCC3387	1	13	9	30	21	4	0	0	3
Dinoflagellata	*Ceratium fusus* PA161109	1	15	10	18	12	9	1	1	3
Dinoflagellata	*Crypthecodinium cohnii* Seligo	1	6	5	15	2	4	0	0	3
Dinoflagellata	*Dinophysis acuminata* DAEP01	4	15	9	29	13	8	0	0	2
Dinoflagellata	*Durinskia baltica* CSIRO_CS 38	2	12	9	18	9	8	0	0	4
Dinoflagellata	*Gambierdiscus australes* CAWD 149	1	5	0	9	14	6	0	0	2
Dinoflagellata	*Glenodinium foliaceum* CCAP1116_3	2	9	3	23	7	6	0	1	4
Dinoflagellata	*Gonyaulax spinifera* CCMP409	1	2	0	10	10	8	1	1	1
Dinoflagellata	*Heterocapsa rotundata* SCCAP K 0483	2	19	4	12	6	4	0	0	6
Dinoflagellata	*Heterocapsa triquestra* CCMP 448	1	8	5	13	5	4	0	0	3
Dinoflagellata	*Karenia brevis* CCMP2229	1	14	8	10	8	7	0	1	4
Dinoflagellata	*Karenia brevis* SP1	1	14	13	16	6	8	0	1	4
Dinoflagellata	*Karenia brevis* SP3	1	12	9	13	8	10	0	1	4
Dinoflagellata	*Karenia brevis* Wilson	1	14	7	14	9	8	0	2	5
Dinoflagellata	*Karlodinium micrum* CCMP2283	2	9	7	46	13	31	2	0	5
Dinoflagellata	*Kryptoperidinium foliaceum* CCMP1326	4	14	11	64	16	10	1	0	7
Dinoflagellata	*Lingulodinium polyedra* CCMP1738	1	17	8	19	11	11	1	0	3
Dinoflagellata	*Noctiluca scintillans* Unknown	1	7	3	9	1	6	0	1	1
Dinoflagellata	*Oxyrrhis marina*	1	2	5	9	7	3	0	1	2
Dinoflagellata	*Oxyrrhis marina* CCMP1795	0	0	0	0	3	0	0	0	0
Dinoflagellata	*Oxyrrhis marina* LB1974	1	2	4	10	4	2	0	0	2
Dinoflagellata	*Pelagodinium beii* RCC1491	1	8	2	12	11	4	0	0	4
Dinoflagellata	*Peridinium aciculiferum* PAER_2	1	7	5	11	6	5	0	0	3
Dinoflagellata	*Polarella glacialis* CCMP 1383	1	28	5	23	5	5	0	0	8

Continued on next page

Supplementary Table 2 – *Continued from previous page*

clade	species	TOP1	TOP2	TOP3	MCM	PCNA	RPA1	RPA2	RPA3	RFC1
Dinoflagellata	*Prorocentrum minimum* CCMP1329	1	15	6	29	13	6	0	0	3
Dinoflagellata	*Prorocentrum minimum* CCMP2233	1	14	4	29	12	5	0	0	3
Dinoflagellata	*Protoceratium reticulatum* CCCM 535 CCMP 1889	2	20	9	18	11	10	0	0	2
Dinoflagellata	*Pyrodinium bahamense* pbaha01	1	21	8	29	19	11	0	0	3
Dinoflagellata	*Scrippsiella hangoei* like SHHI_4	1	8	6	22	6	16	0	2	2
Dinoflagellata	*Scrippsiella hangoei* SHTV5	1	8	11	14	3	5	0	0	2
Dinoflagellata	*Scrippsiella trochoidea* CCMP3099	1	27	10	38	12	8	1	1	3
Dinoflagellata	*Symbiodinium kawagutii* CCMP2468	0	0	0	0	2	0	0	0	0
Dinoflagellata	*Symbiodinium* sp. C1	1	9	4	9	6	4	0	0	3
Dinoflagellata	*Symbiodinium* sp. C15	1	7	2	12	3	4	1	0	3
Dinoflagellata	*Symbiodinium* sp. CCMP2430	1	7	2	10	7	4	0	0	3
Dinoflagellata	*Symbiodinium* sp. Mp	1	7	3	13	6	3	0	0	3
Dinoflagellata	*Togula jolla* CCCM 725	1	17	3	21	3	6	0	0	4
Discosea	*Mayorella* sp. BSH 02190019	1	3	2	5	1	1	0	1	1
Discosea	*Neoparamoeba aestuarina* SoJaBio B1 5 56 2	3	3	3	12	3	3	0	1	1
Discosea	*Paramoeba atlantica* 621 1 CCAP 1560 9	1	3	2	8	3	2	0	1	1
Discosea	*Pessonella* sp. PRA 29	1	1	3	0	1	5	0	2	3
Discosea	*Stygamoeba regulata* BSH 02190019	3	8	2	7	2	4	0	0	2
Discosea	*Trichosphaerium* sp. Am I 7 wt	2	0	0	1	2	3	0	0	2
Eugelnophyta	*Eutreptiella gymnastica* like CCMP1594	1	1	1	5	2	1	0	1	1
Foraminifera	*Ammonia* sp. Unknown	1	1	3	9	5	2	0	1	1
Foraminifera	*Elphidium margaritaceum* Unknown	1	1	2	8	3	1	1	0	1
Foraminifera	*Rosalina* sp. Unknown	1	0	0	9	5	0	2	0	1
Foraminifera	*Sorites* sp. Unknown	3	3	0	27	12	3	0	0	2
Fungi	*Debaryomyces hansenii* J26	1	0	0	4	0	0	0	0	1
Glaucophyte	*Gloeochaete witrockiana* SAG46_84	2	2	3	9	2	2	1	1	1
Haptophyte	*Calcidiscus leptoporus* RCC1130	1	3	0	7	1	1	1	0	1
Haptophyte	*Chrysochromulina brevifilum* UTEX LB 985	1	2	1	4	1	3	0	1	0
Haptophyte	*Chrysochromulina ericina* CCMP281	2	1	0	10	1	3	1	1	2
Haptophyte	*Chrysochromulina polylepis* CCMP1757	1	3	5	9	1	2	1	1	1
Haptophyte	*Chrysoculter rhomboideus* RCC1486	1	0	0	9	1	0	0	1	0
Haptophyte	*Coccolithus pelagicus* ssp *braarudi* PLY182g	1	3	0	7	1	2	1	1	0
Haptophyte	*Emiliania huxleyi* 374	1	2	1	9	1	1	0	0	0
Haptophyte	*Emiliania huxleyi* 379	1	1	1	0	0	2	0	0	0
Haptophyte	*Emiliania huxleyi* CCMP370	1	3	5	9	0	2	1	1	1
Haptophyte	*Emiliania huxleyi* PLYM219	1	3	4	10	0	2	1	1	1
Haptophyte	*Exanthemachrysis gayraliae* RCC1523	1	2	0	1	1	1	0	1	1
Haptophyte	*Gephyrocapsa oceanica* RCC1303	1	3	5	11	1	1	0	0	1
Haptophyte	*Imantonia* sp. RCC918	3	1	1	4	2	1	1	1	0
Haptophyte	*Isochrysis galbana* CCMP1323	2	5	6	13	2	3	1	0	2
Haptophyte	*Isochrysis* sp. CCMP1244	1	2	5	11	1	1	0	1	1
Haptophyte	*Isochrysis* sp. CCMP1324	1	2	0	12	1	2	1	0	1
Haptophyte	*Pavlova* sp. CCMP459	1	2	1	6	2	1	2	1	1
Haptophyte	*Phaeocystis antarctica* Caron Lab Isolate	3	7	2	12	1	3	2	0	2
Haptophyte	*Phaeocystis* sp. CCMP2710	1	0	1	2	1	1	1	1	1
Haptophyte	*Pleurochrysis carterae* CCMP645	3	2	1	7	1	2	1	1	1
Haptophyte	*Prymnesium parvum* Texoma1	1	6	4	1	1	2	1	1	1
Haptophyte	*Scyphosphaera apsteinii* RCC1455	1	3	1	7	1	2	1	0	1
Heterolobosea	*Percolomonas cosmopolitus* AE 1 ATCC 50343	1	4	2	9	2	2	0	0	1
Heterolobosea	*Percolomonas cosmopolitus* WS	1	3	1	12	1	2	0	0	3
Khakista	*Corethron pennatum* L29A3	2	5	5	16	1	1	1	0	1
Khakista	*Detonula confervacea* CCMP 353	1	3	2	9	1	1	2	1	1
Kinetoplastida	*Neobodo designis* CCAP 1951 1	1	1	4	8	1	1	0	0	1
Labyrinthulida	*Aplanochytrium* sp. PBS07	1	2	1	3	1	1	1	2	1
Labyrinthulida	*Aplanochytrium stocchinoi* GSBS06	1	2	0	7	1	1	1	1	1
Pelagophyte	*Aureococcus anophagefferens* CCMP1850	6	2	3	45	1	2	0	0	1
Pelagophyte	*Aureoumbra lagunensis* CCMP1510	1	2	2	9	1	2	1	0	1
Pelagophyte	*Chrysocystis fragilis* CCMP3189	2	0	2	6	1	1	1	0	1

Continued on next page

Supplementary Table 2 – *Continued from previous page*

clade	species	TOP1	TOP2	TOP3	MCM	PCNA	RPA1	RPA2	RPA3	RFC1
Pelagophyte	*Chrysoreinhardia* sp. CCMP2950	1	2	1	5	0	1	0	0	1
Pelagophyte	*Chrysoreinhardia* sp. CCMP3193	1	3	2	10	1	2	1	0	1
Pelagophyte	*Pelagomonas calceolata* CCMP1756	1	2	1	9	1	1	2	0	1
Pelagophyte	*Sarcinochrysis* sp. CCMP770	0	0	0	2	1	1	1	1	0
Perkinsid	*Perkinsus chesapeaki* ATCC_PRA_65	2	0	0	0	0	0	0	0	0
Perkinsid	*Perkinsus marinus* ATCC50439	1	0	0	1	2	0	0	0	0
Pinguiophyte	*Phaeomonas parva* CCMP2877	1	3	1	5	3	1	0	1	0
Pinguiophyte	*Pinguiococcus pyrenoidosus* CCMP2078	1	2	3	0	1	1	0	1	0
Raphidophyte	*Chattonella subsalsa* CCMP2191	1	3	0	5	1	1	1	0	1
Raphidophyte	*Fibrocapsa japonica* CCMP1661	0	1	1	5	1	1	0	1	0
Raphidophyte	*Heterosigma akashiwo* CCMP2393	1	4	2	11	2	1	0	1	1
Raphidophyte	*Heterosigma akashiwo* CCMP3107	1	7	2	0	1	1	0	0	0
Raphidophyte	*Heterosigma akashiwo* CCMP452	0	1	0	4	1	1	0	0	0
Raphidophyte	*Heterosigma akashiwo* NB	1	6	1	8	1	1	0	1	1
Rhodophyte	*Compsopogon coeruleus* SAG 36.94	1	3	2	11	1	1	0	0	1
Rhodophyte	*Erythrolobus australicus* CCMP3124	1	2	3	0	1	1	0	1	1
Rhodophyte	*Erythrolobus madagascarensis* CCMP3276	1	1	1	3	1	2	0	1	0
Rhodophyte	*Madagascaria erythrocladiodes* CCMP3234	3	4	5	12	1	2	0	1	2
Rhodophyte	*Porphyridium aerugineum* SAG 1380 2	2	1	2	5	1	2	1	0	1
Rhodophyte	*Rhodella maculata* CCMP736	1	3	3	12	1	1	0	0	1
Rhodophyte	*Rhodosorus marinus* CCMP 769	1	8	6	17	0	3	0	0	2
Rhodophyte	*Timspurckia oligopyrenoides* CCMP3278	1	2	4	6	1	2	1	1	1
Silicoflagellates	*Dictyocha speculum* CCMP1381	1	4	2	9	1	2	1	1	1
Silicoflagellates	*Pseudopedinella elastica* CCMP716	1	5	6	9	1	1	1	1	1
Silicoflagellates	*Pteridomonas danica* PT	1	1	1	2	1	1	1	1	0
Silicoflagellates	*Rhizochromulina marina* cf CCMP1243	1	5	2	8	2	2	1	1	1
Synchromophyceae	*Synchroma pusillum* CCMP3072	1	0	1	3	3	1	0	1	1
Syndinian	*Amoebophrya* sp. Ameob2	2	8	1	13	0	1	0	0	0
Thraustochytrid	*Aurantiochytrium limacinum* ATCCMYA1381	1	3	2	9	1	1	0	1	1
Thraustochytrid	*Schizochytrium aggregatum* ATCC28209	1	1	1	4	1	1	0	0	1
Thraustochytrid	*Thraustochytrium* sp. LLF1b	1	2	1	9	1	1	0	1	1
Tubulinid	*Filamoeba nolandi* NC AS 23 1	2	4	1	13	0	3	1	0	1
Tubulinid	*Sexangularia* sp. ATCC50979	0	6	7	14	2	2	1	0	3
Vanellinid	*Vannella robusta* DIVA3 518 3 11 1 6	1	2	3	6	1	2	1	1	1
Vanellinid	*Vannella* sp. DIVA3 517 6 12	6	6	9	13	1	1	0	1	1
Xantophyte	*Vaucheria litorea* CCMP2940	1	2	0	6	1	1	0	1	1

Supplementary Figures

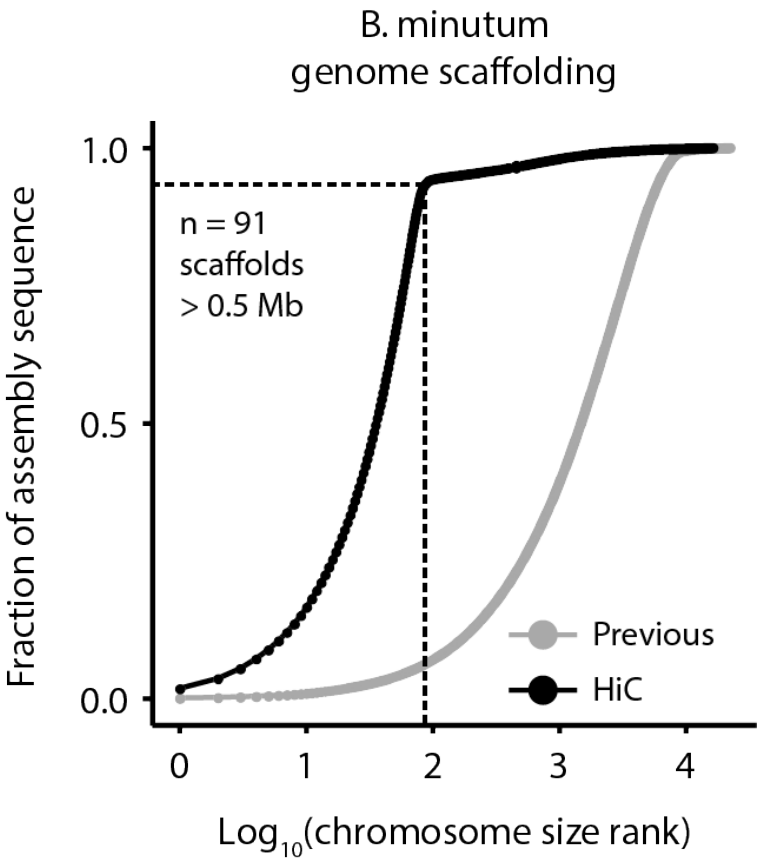

Supplementary Figure 1: Cumulative distribution of scaffolds and pseudochromosome sizes before and after Hi-C scaffolding of the draft *Breviolum minutum* assembly[9]. 3D DNA[27] scaffolding of the assembly results in 91 major pseudochromosomes ≥500kb encompassing ∼94% of the assembled sequence.

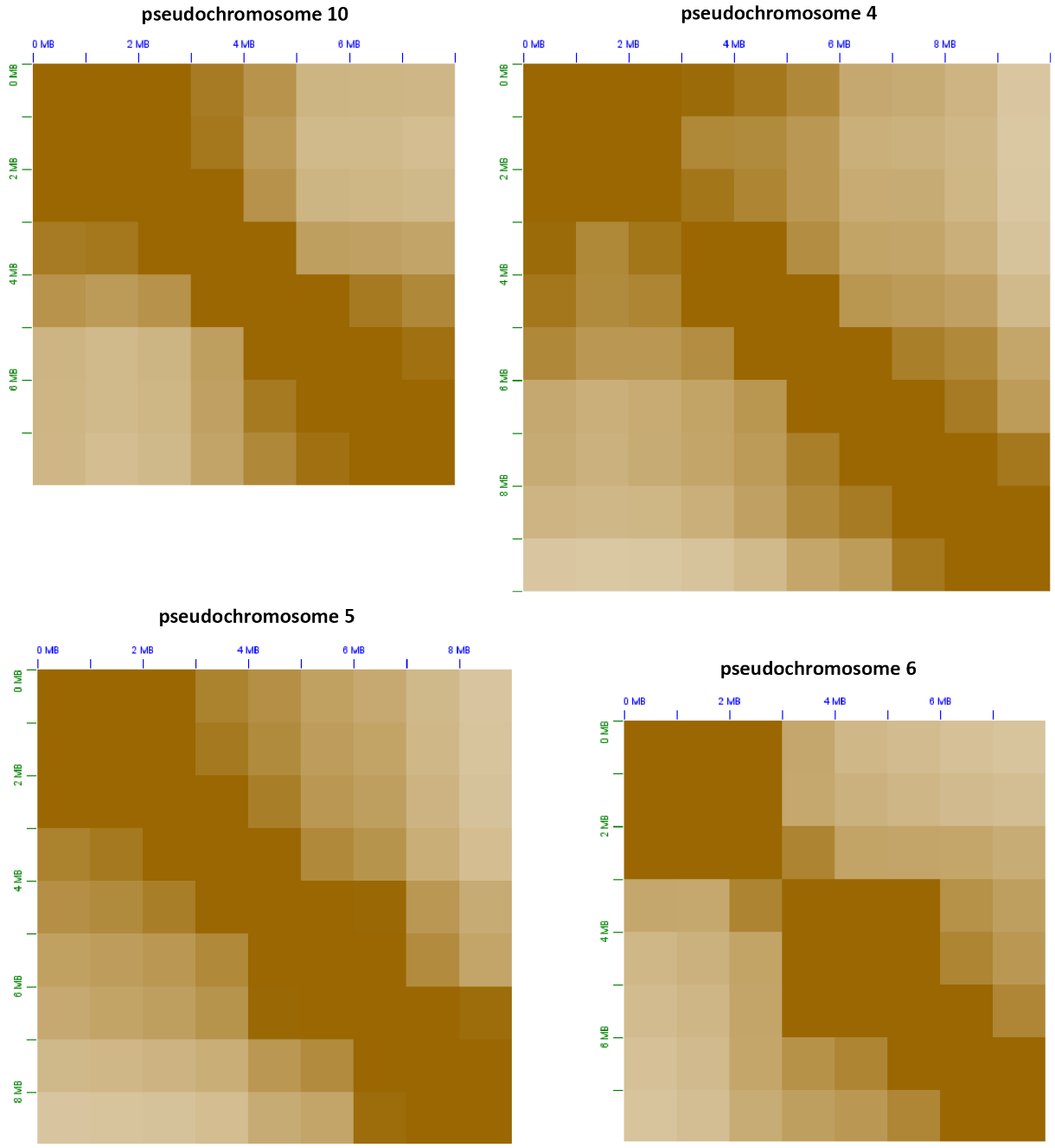

Supplementary Figure 2: Broad-level bipartite to tripartite topological structure of dinoflagellate chromosomes. Shown are 1Mbp-resolution KR-normalized[35] Hi-C matrices for four of the *B. minutum* pseudochromosomes.

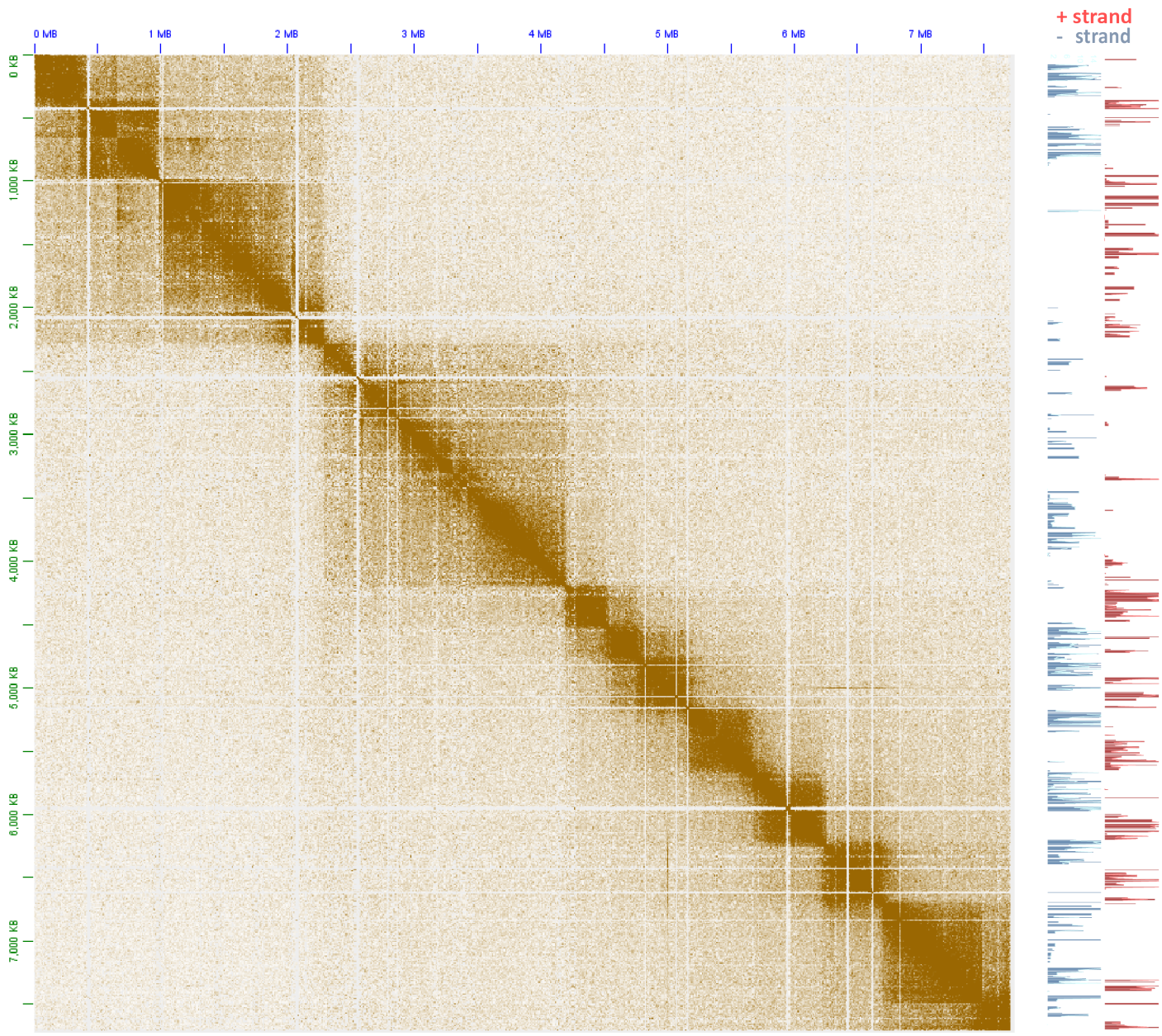

Supplementary Figure 3: The topological domain organization of dinoflagellate chromosomes is related to tandem gene array orientation. Shown is the 5kb-resolution KR-normalized Hi-C map together with strand-specific RNA expression levels for pseudochromosome 17.

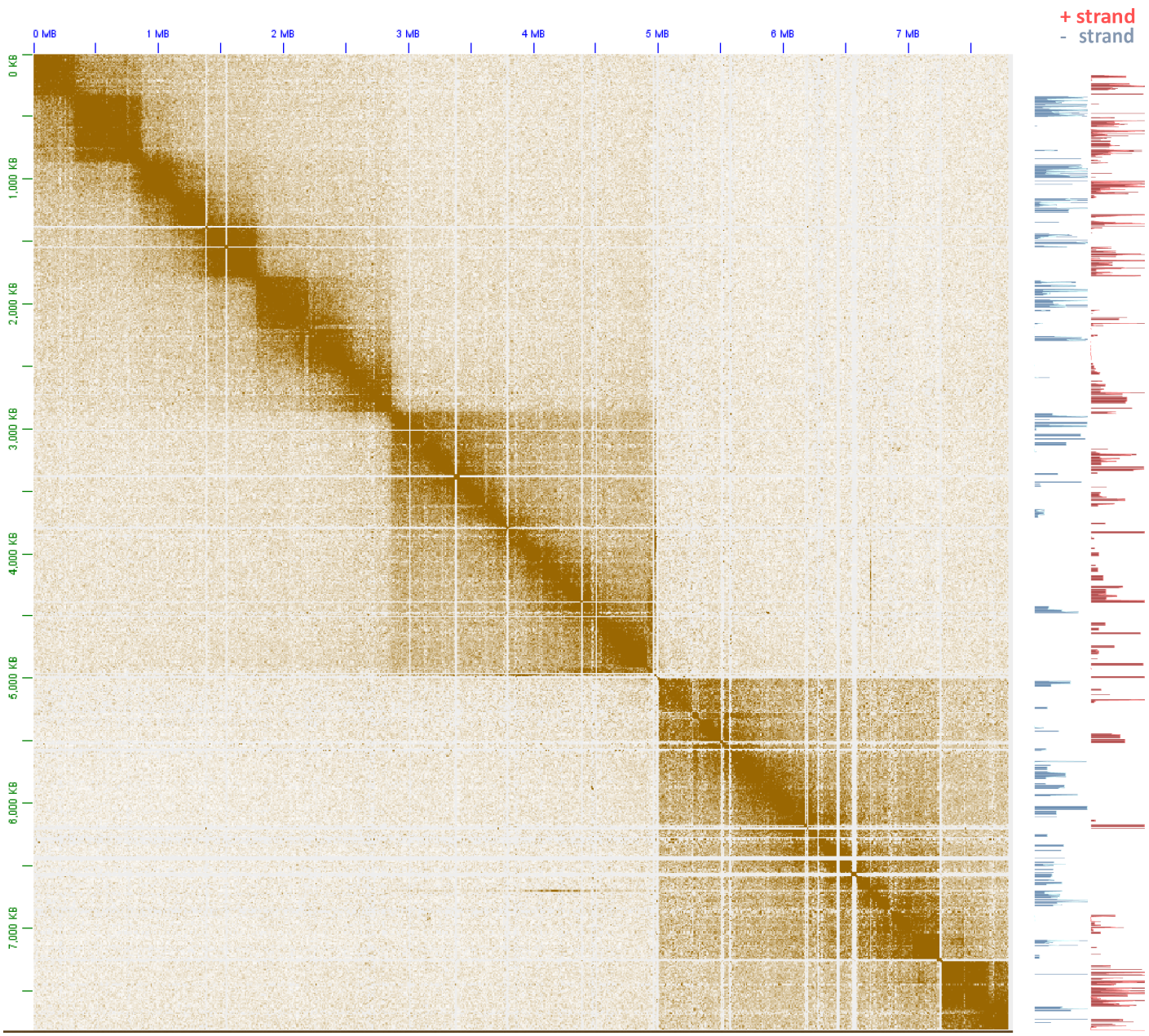

Supplementary Figure 4: The topological domain organization of dinoflagellate chromosomes is related to tandem gene array orientation. Shown is the 5kb-resolution KR-normalized Hi-C map together with strand-specific RNA expression levels for pseudochromosome 18.

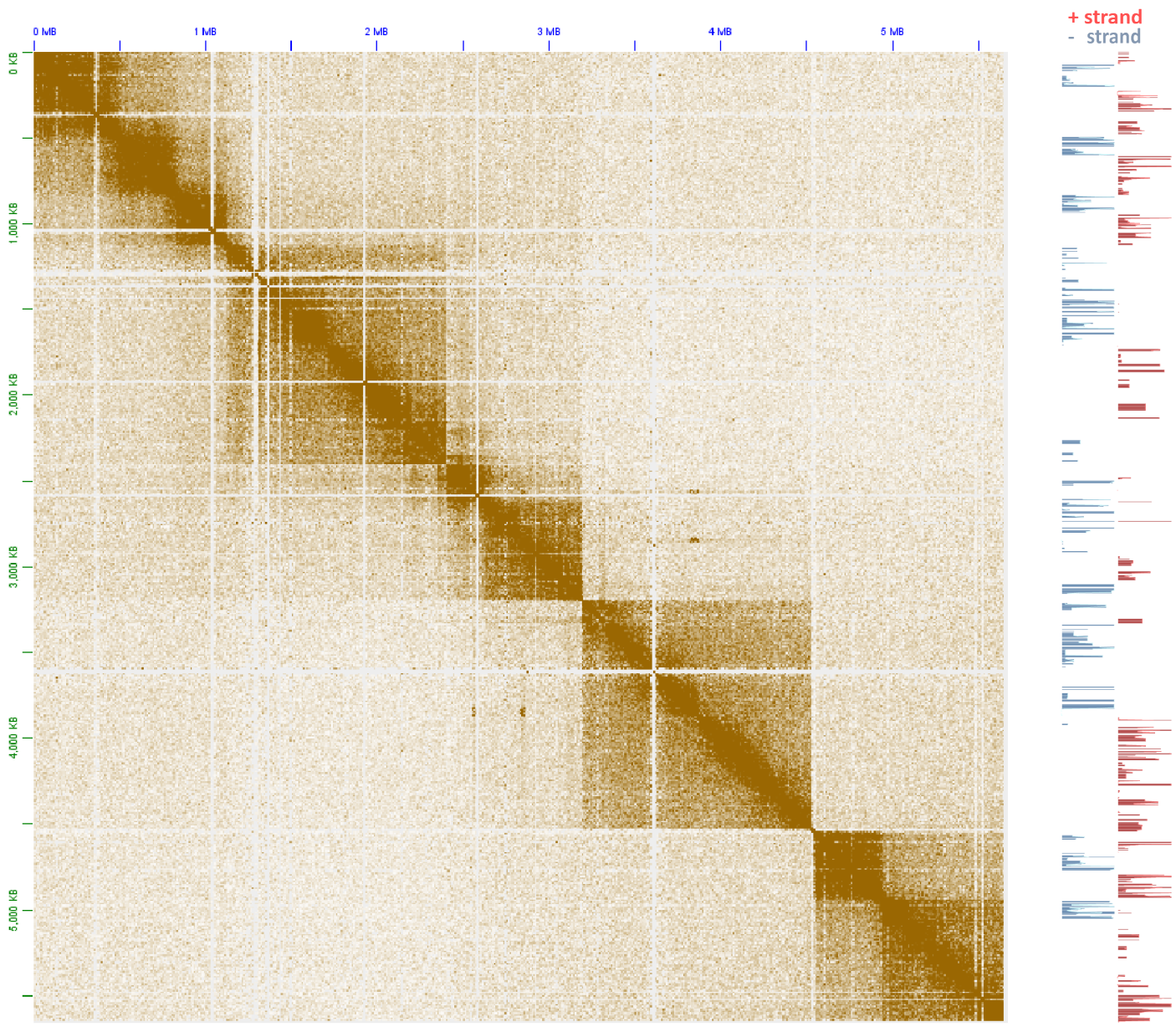

Supplementary Figure 5: The topological domain organization of dinoflagellate chromosomes is related to tandem gene array orientation. Shown is the 5kb-resolution KR-normalized Hi-C map together with strand-specific RNA expression levels for pseudochromosome 21.

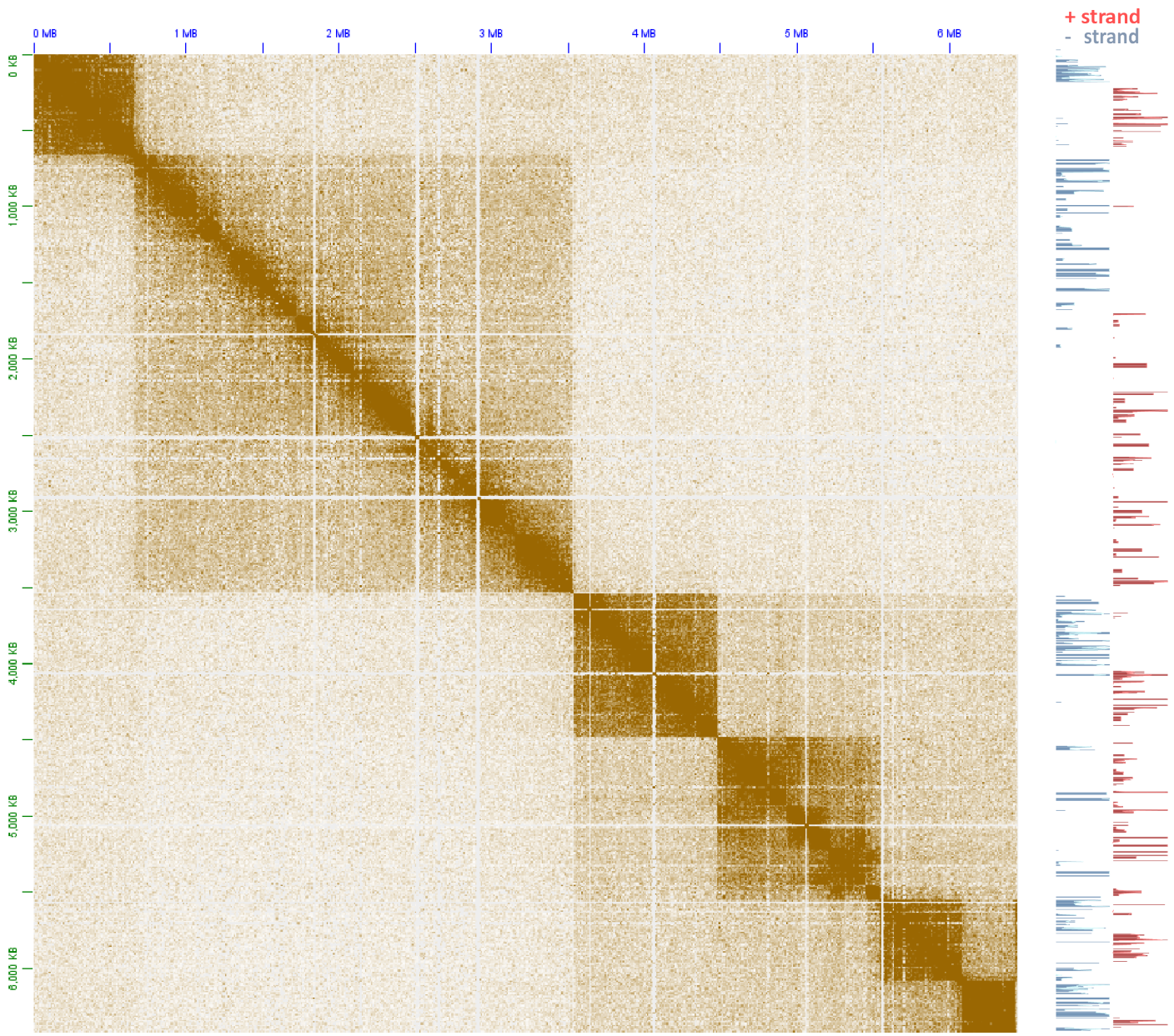

Supplementary Figure 6: The topological domain organization of dinoflagellate chromosomes is related to tandem gene array orientation. Shown is the 5kb-resolution KR-normalized Hi-C map together with strand-specific RNA expression levels for pseudochromosome 26.

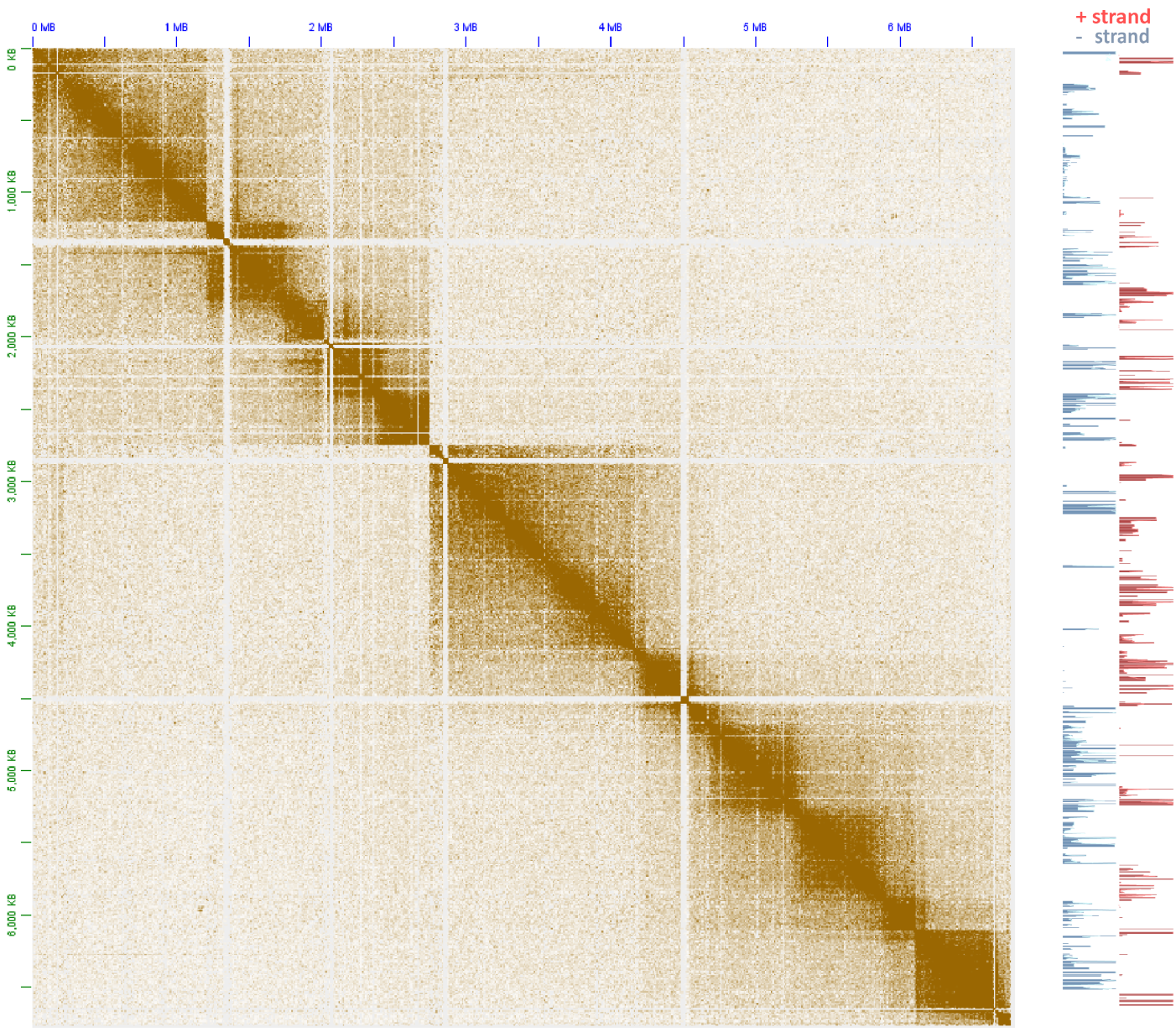

Supplementary Figure 7: The topological domain organization of dinoflagellate chromosomes is related to tandem gene array orientation. Shown is the 5kb-resolution KR-normalized Hi-C map together with strand-specific RNA expression levels for pseudochromosome 32.

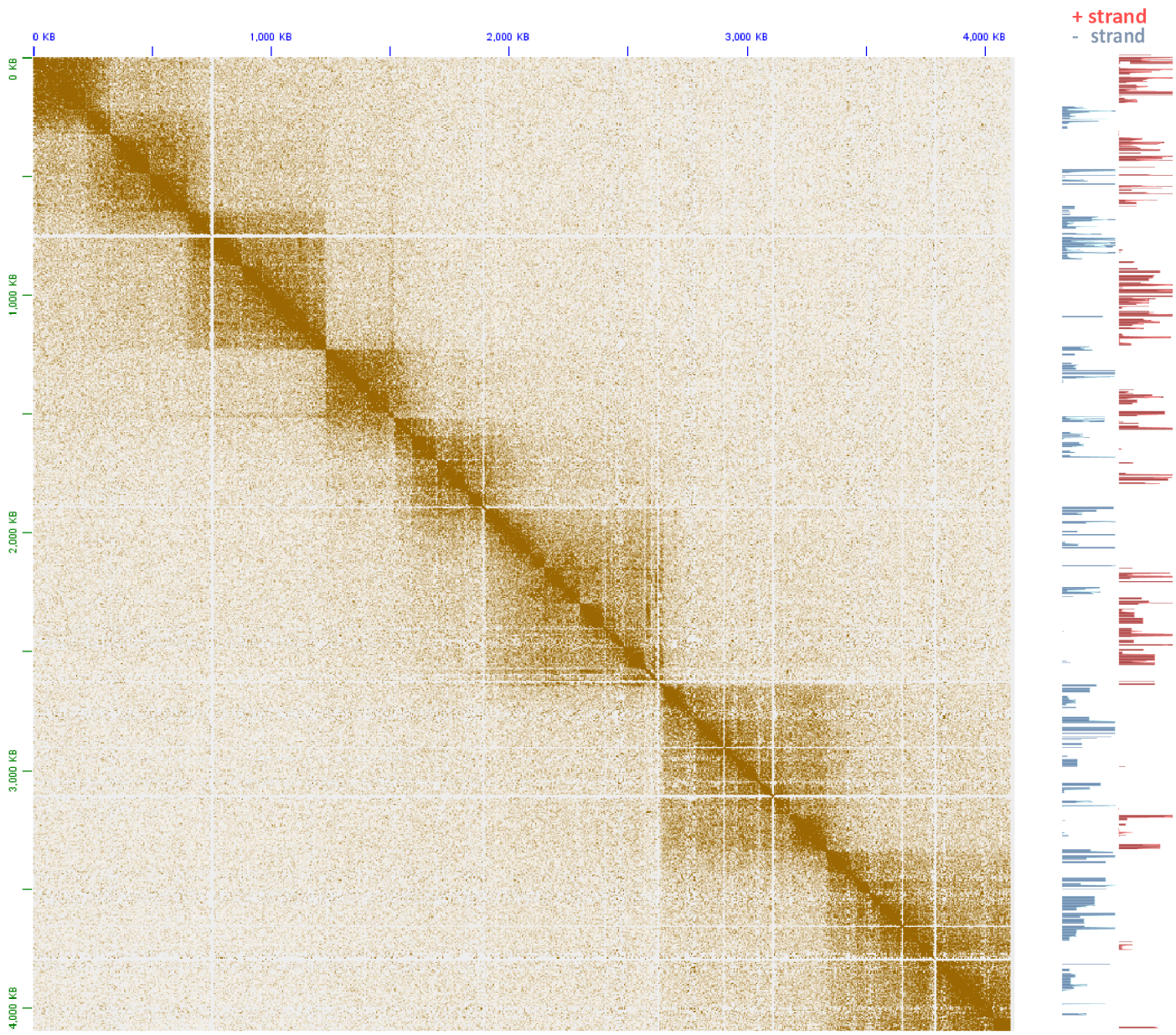

Supplementary Figure 8: The topological domain organization of dinoflagellate chromosomes is related to tandem gene array orientation. Shown is the 5kb-resolution KR-normalized Hi-C map together with strand-specific RNA expression levels for pseudochromosome 36.

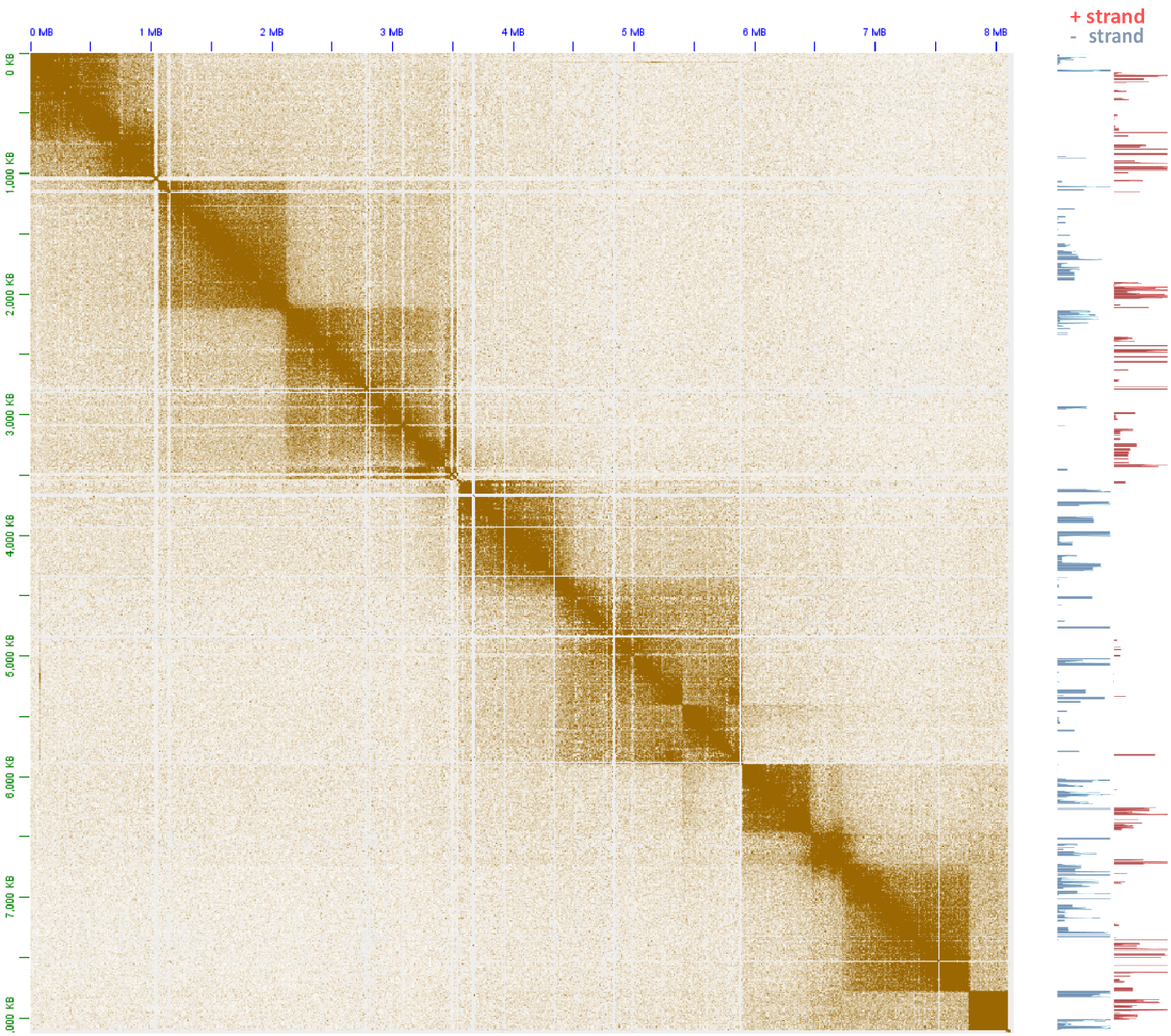

Supplementary Figure 9: The topological domain organization of dinoflagellate chromosomes is related to tandem gene array orientation. Shown is the 5kb-resolution KR-normalized Hi-C map together with strand-specific RNA expression levels for pseudochromosome 71.

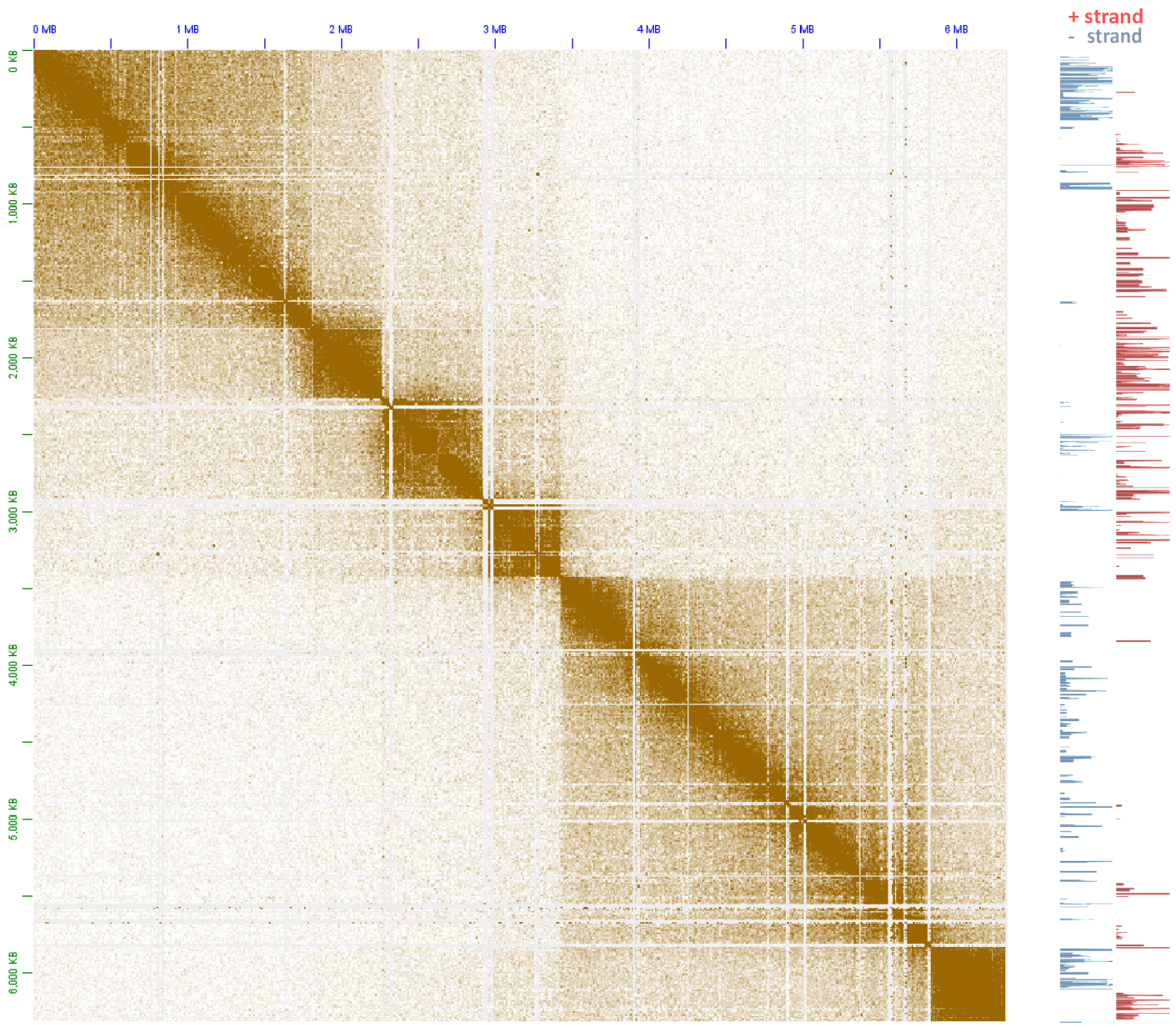

Supplementary Figure 10: The topological domain organization of dinoflagellate chromosomes is related to tandem gene array orientation. Shown is the 5kb-resolution KR-normalized Hi-C map together with strand-specific RNA expression levels for pseudochromosome 77.

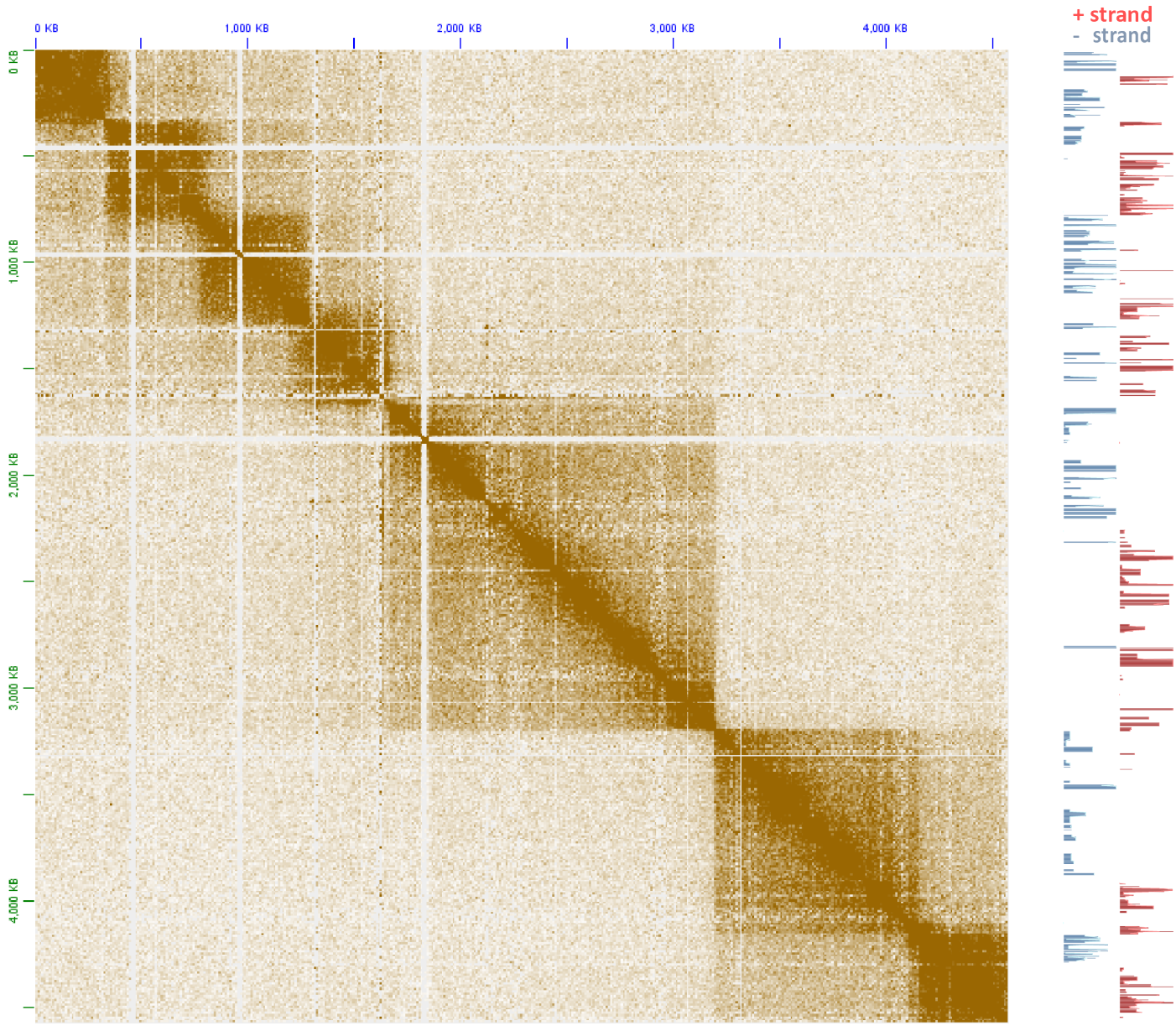

Supplementary Figure 11: The topological domain organization of dinoflagellate chromosomes is related to tandem gene array orientation. Shown is the 5kb-resolution KR-normalized Hi-C map together with strand-specific RNA expression levels for pseudochromosome 78.

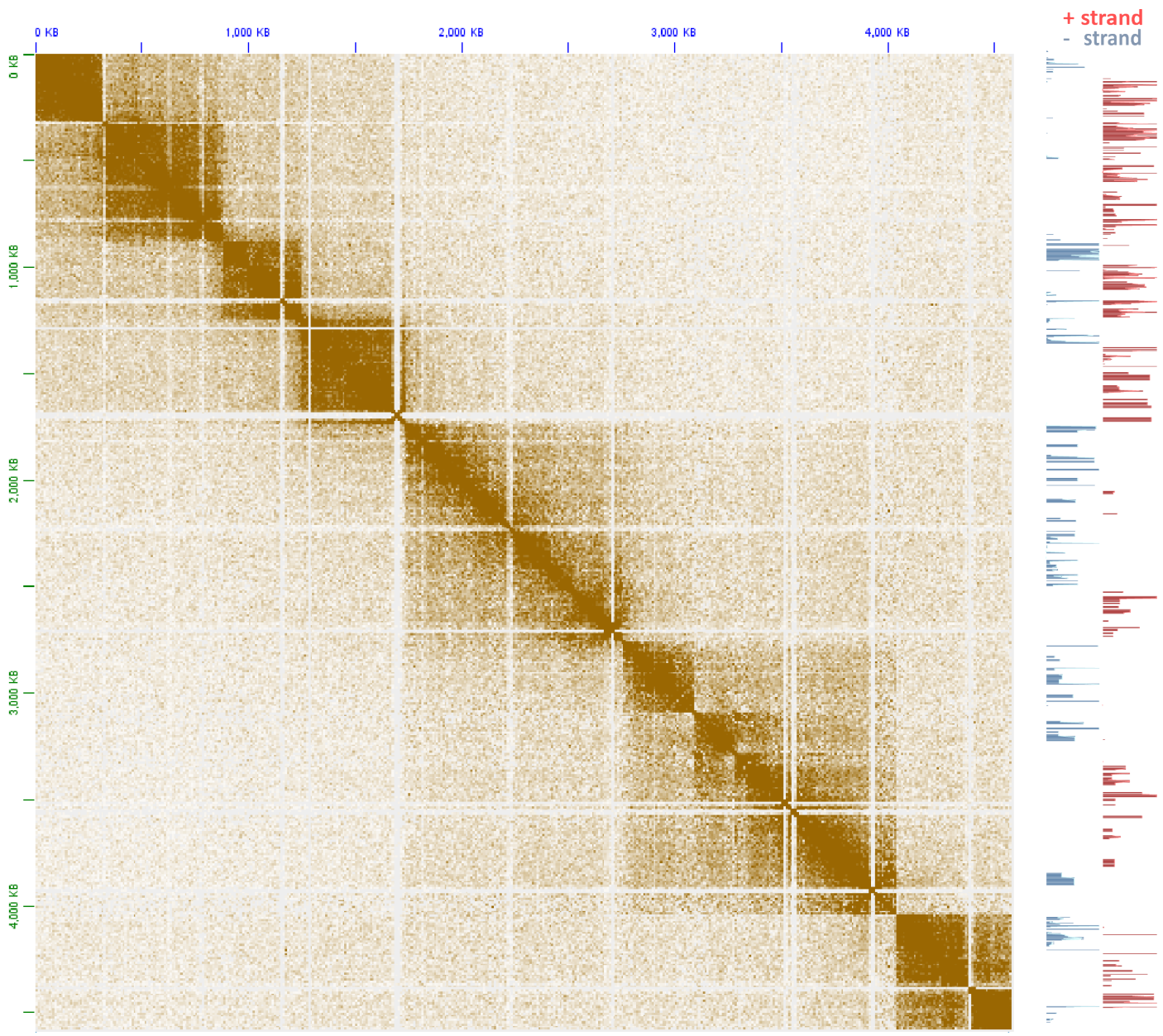

Supplementary Figure 12: The topological domain organization of dinoflagellate chromosomes is related to tandem gene array orientation. Shown is the 5kb-resolution KR-normalized Hi-C map together with strand-specific RNA expression levels for pseudochromosome 88.

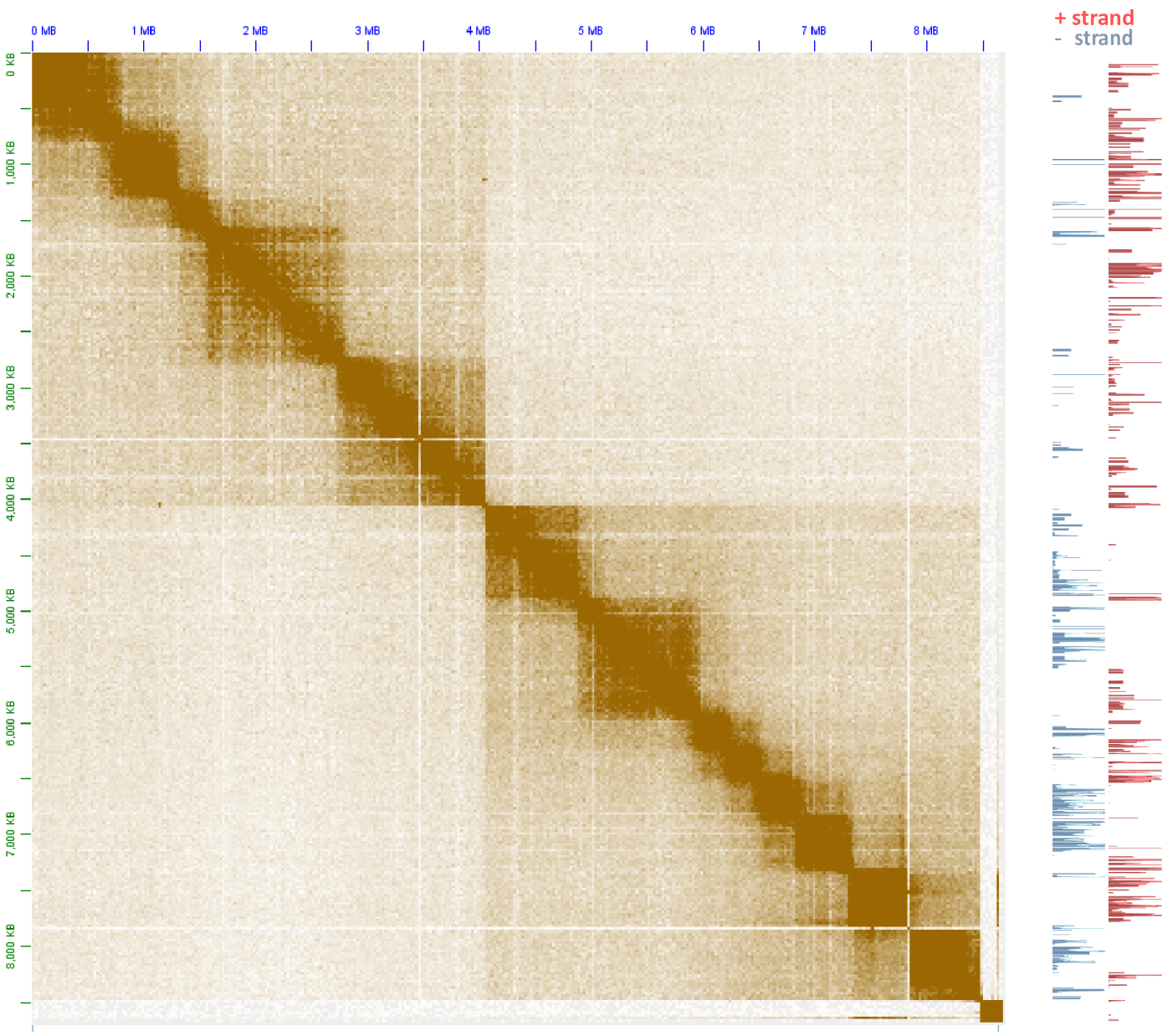

Supplementary Figure 13: The topological domain organization of dinoflagellate chromosomes is related to tandem gene array orientation. Shown is the 5kb-resolution KR-normalized Hi-C map together with strand-specific RNA expression levels for pseudochromosome 89.

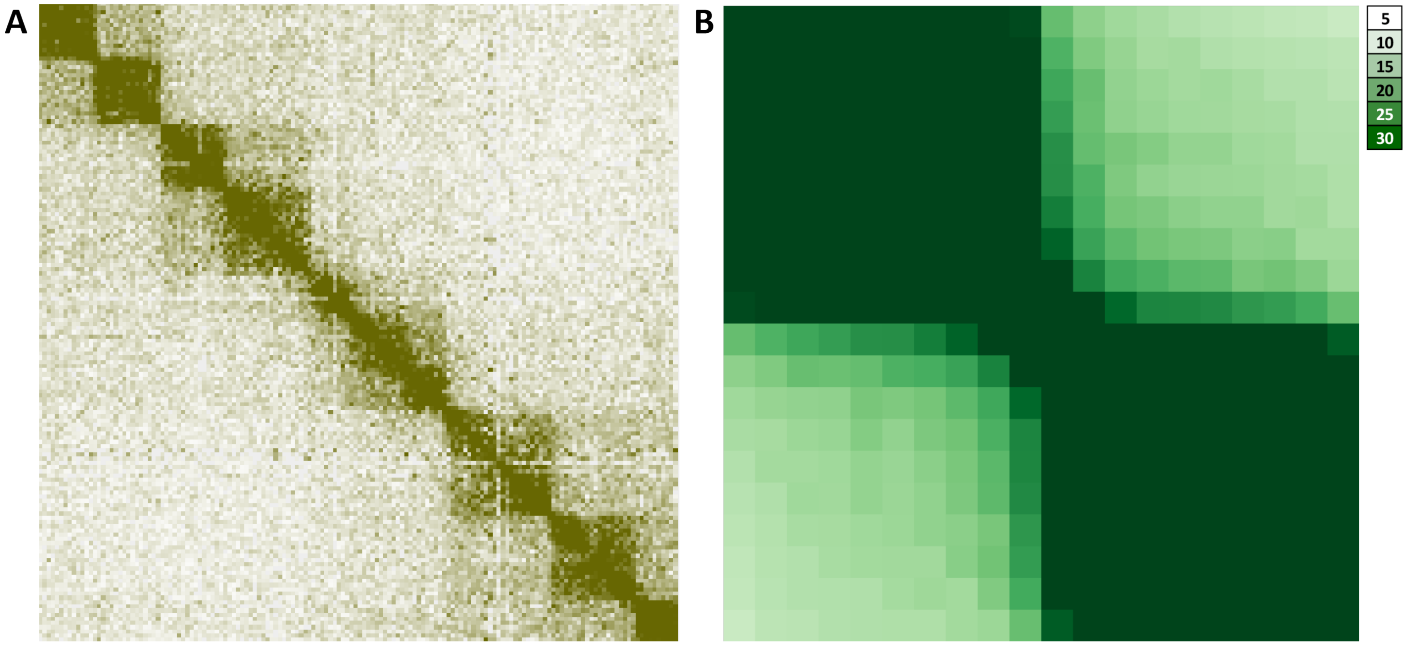

Supplementary Figure 14: DinoTADs become more strongly defined in Hi-C datasets generated by omitting the SDS denaturation step (sample "L1859" in Supplementary Table 1). (A) Snapshot of pseudochromosome 10 at 50-kbp resolution. (B) Metaplot across all dinoTAD boundaries at 50-kbp resolution (drawn to same scale as metaplots in main figures and elsewhere in the supplement)

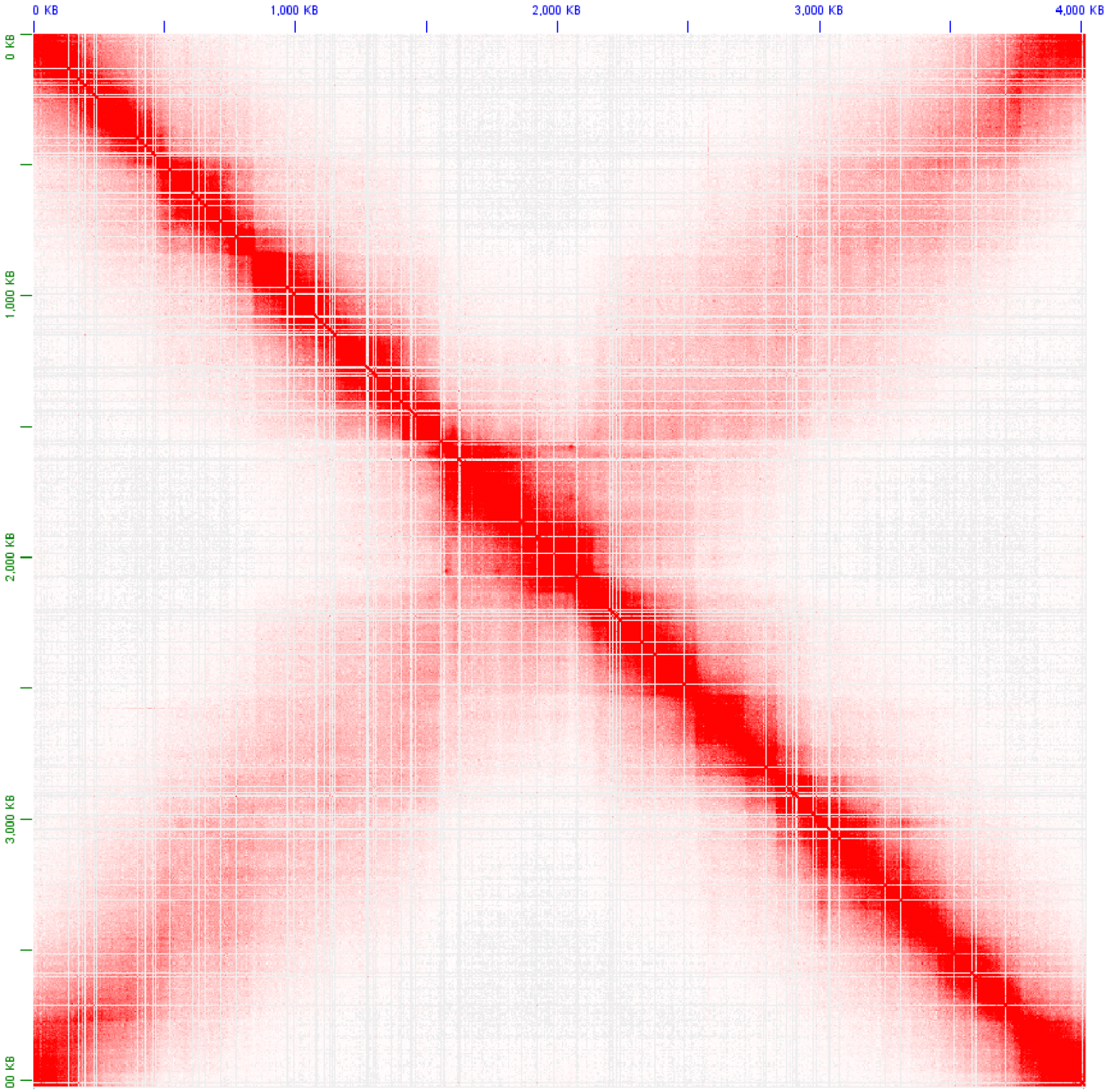

Supplementary Figure 15: Topological structure of the *Caulobacter crescentus* CB15 genome. Shown is the KR-normalized 5-kb resolution maps for the whole *Caulobacter* chromosome (GEO accession GSM1120448).

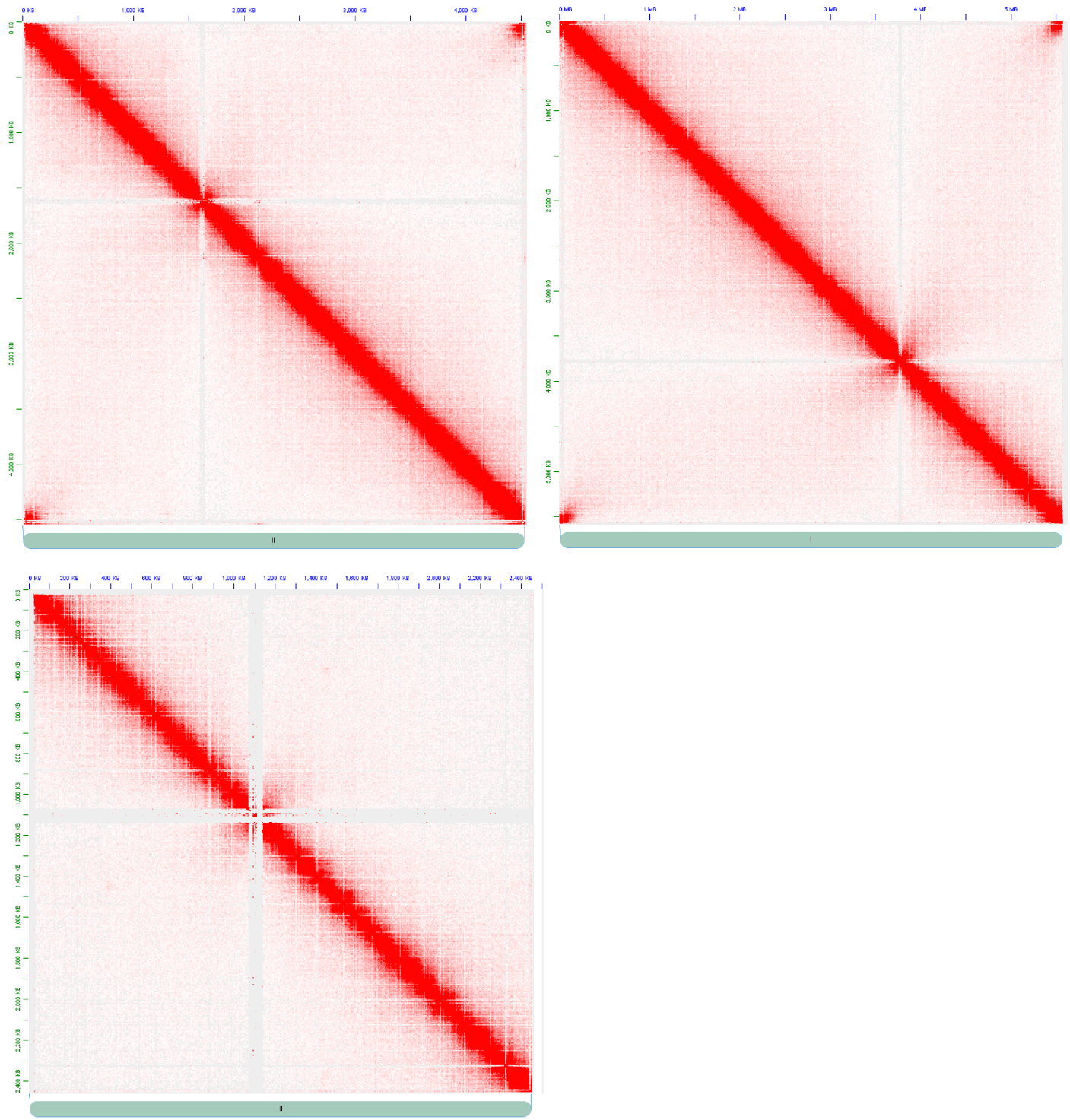

Supplementary Figure 16: Topological structure of the *Schizosaccharomyces pombe* genome. Shown are the KR-normalized 5-kb resolution maps for all three *S. pombe* chromosome (GEO accession GSM1379427).

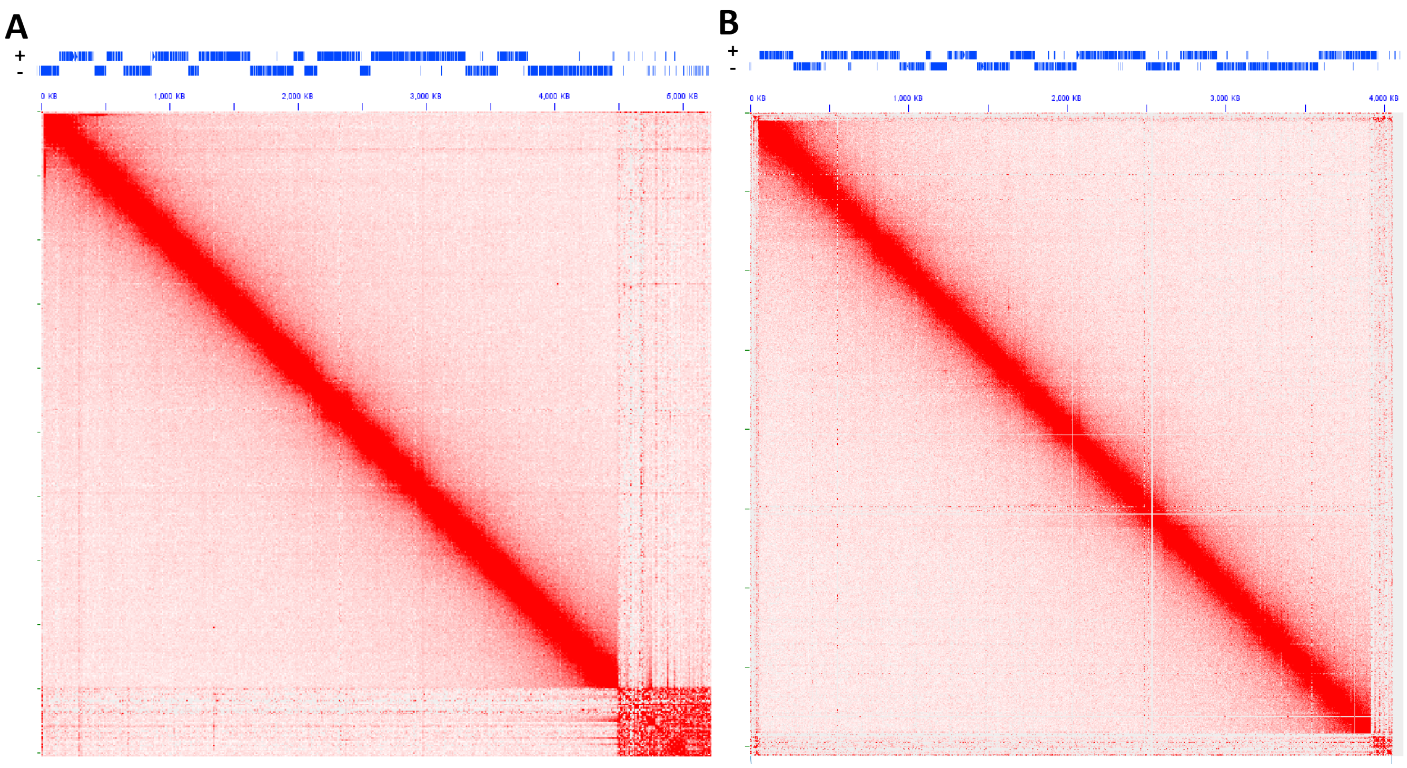

Supplementary Figure 17: No topological domains associated with gene arrays are observed in the kinetoplastid *Trypanosoma brucei*. Shown are KR-normalized 10-kb resolution maps for chr11 (A) and chr10 (B) for GEO accession GSM3346690.

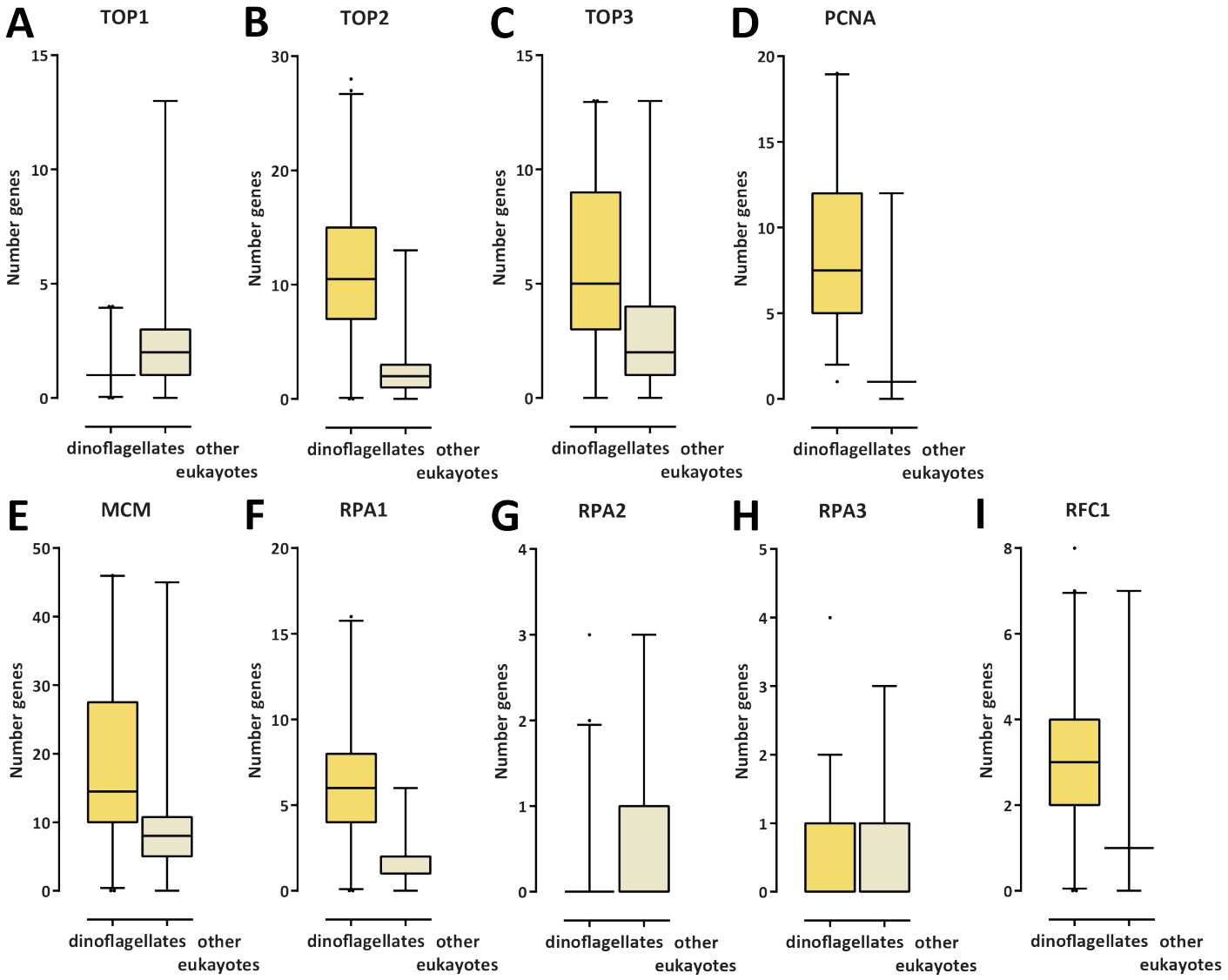

Supplementary Figure 18: Expansion of the Type II and II topoisomerase gene repertoire as well as of certain other replication-related (see Hou et al.[36] for more details) proteins in dinoflagellates. Shown are the number of genes annotated in MMETSP transcriptome assemblies of dinoflagellates and other eukaryotes. (A) Number of Type I topoisomerase genes; (B) Number of Type II topoisomerase genes; (C) Number of Type III topoisomerase genes; (D) Number of PCNA genes; (E) Number of MCM genes; (F) Number of RPA1 genes; (G) Number of RPA2 genes; (H) Number of RPA3 genes; (I) Number of RFC1 genes. Box plots show the 25th, 50th and 75th percentiles, whiskers show the 5-95% intervals. The dinoflagellate (n=41) and non-dinoflagellate (n=243) species shown are the ones from Supplementary Table 2.

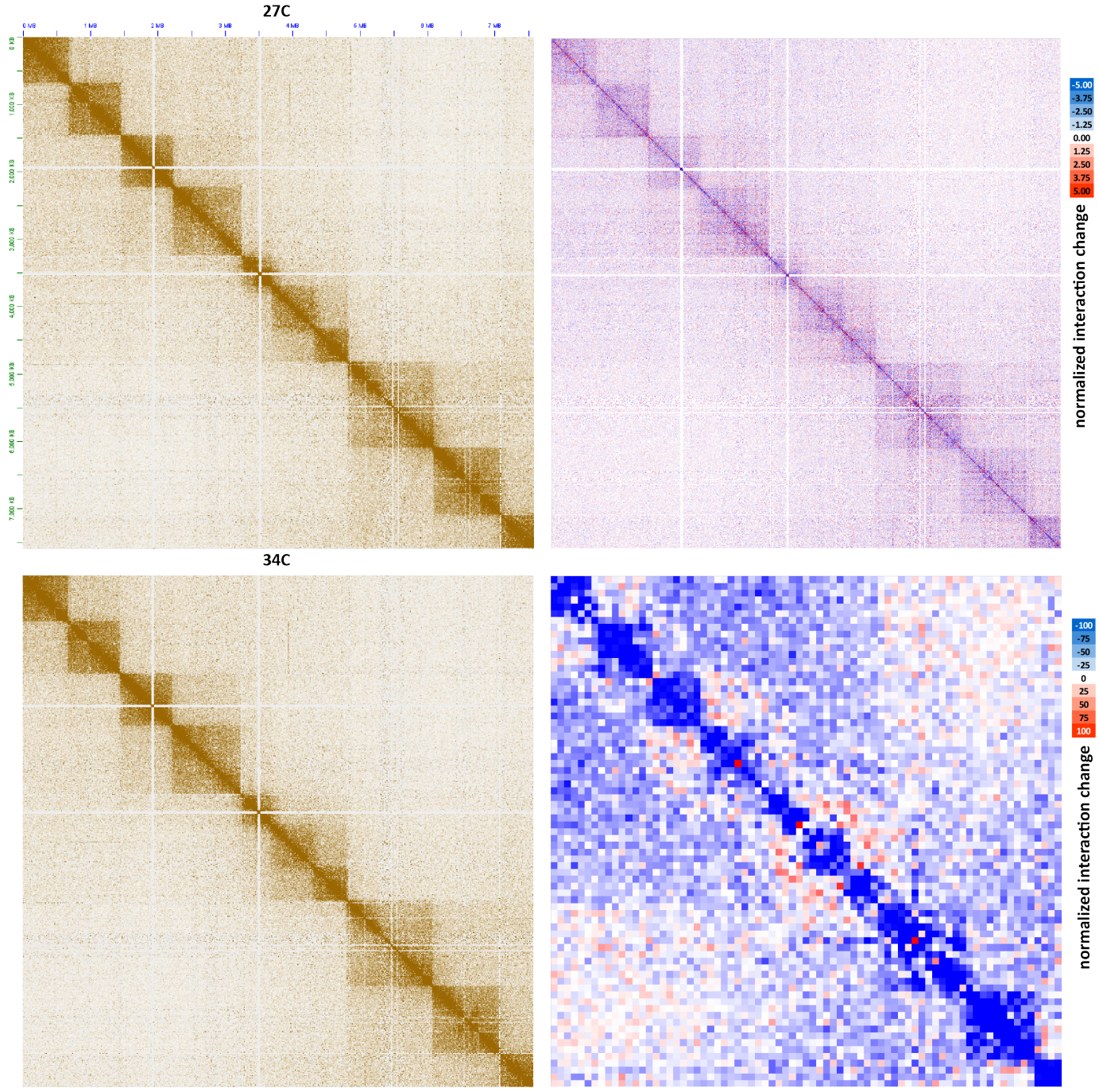

Supplementary Figure 19: Moderate decompaction of dinoTADs upon exposure to elevated temperatures. Shown is pseudochromosome 10 (KR-normalized) and the difference between the KR-normalized Hi-C maps generated from *B. minutum* grown at 34 °C and at 27 °C at 100-kb resolution (lower right) and 5-kb resolution (upper right).

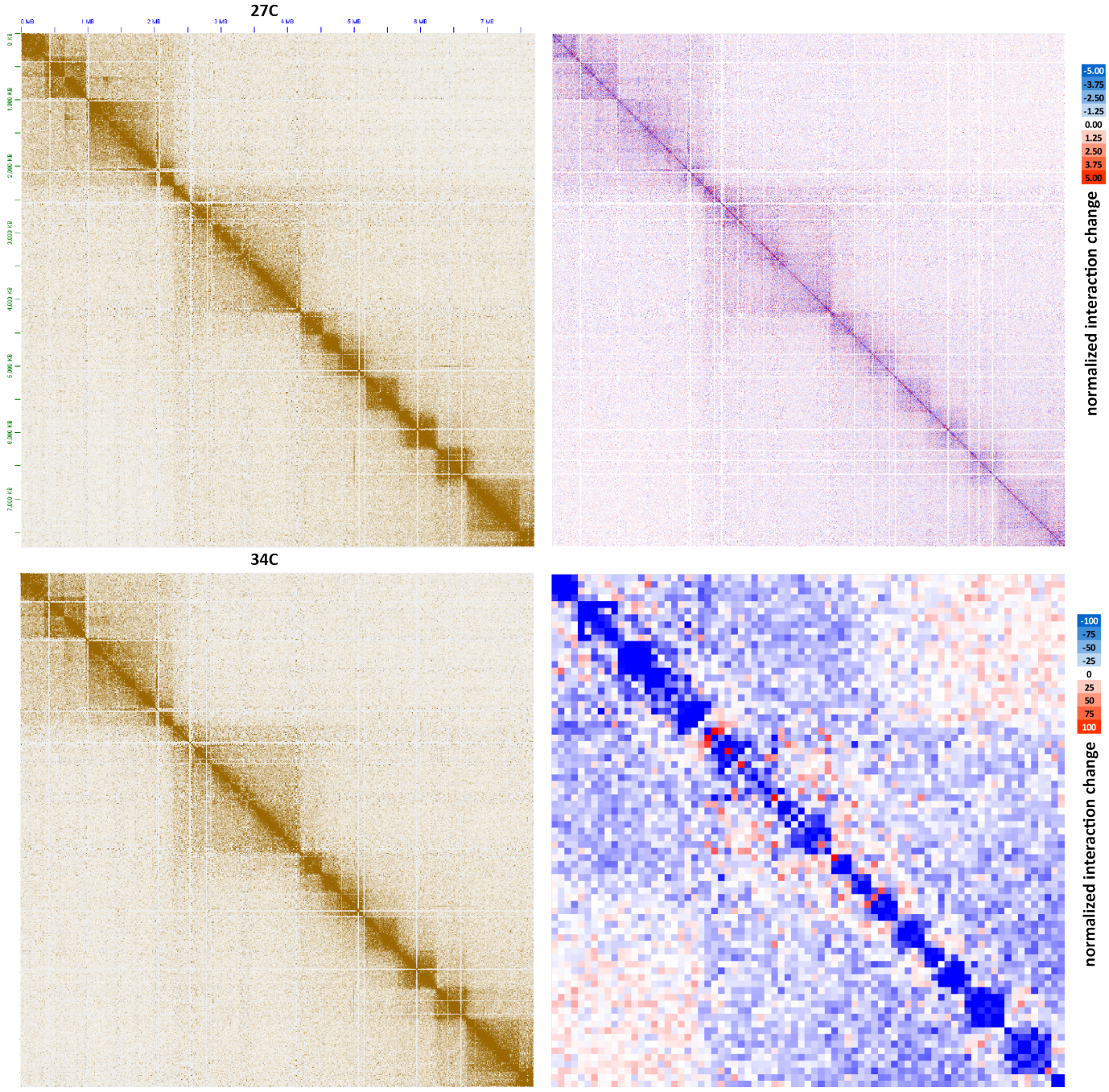

Supplementary Figure 20: Moderate decompaction of dinoTADs upon exposure to elevated temperatures. Shown is pseudochromosome 17 (KR-normalized) and the difference between the KR-normalized Hi-C maps generated from *B. minutum* grown at 34 °C and at 27 °C at 100-kb resolution (lower right) and 5-kb resolution (upper right).

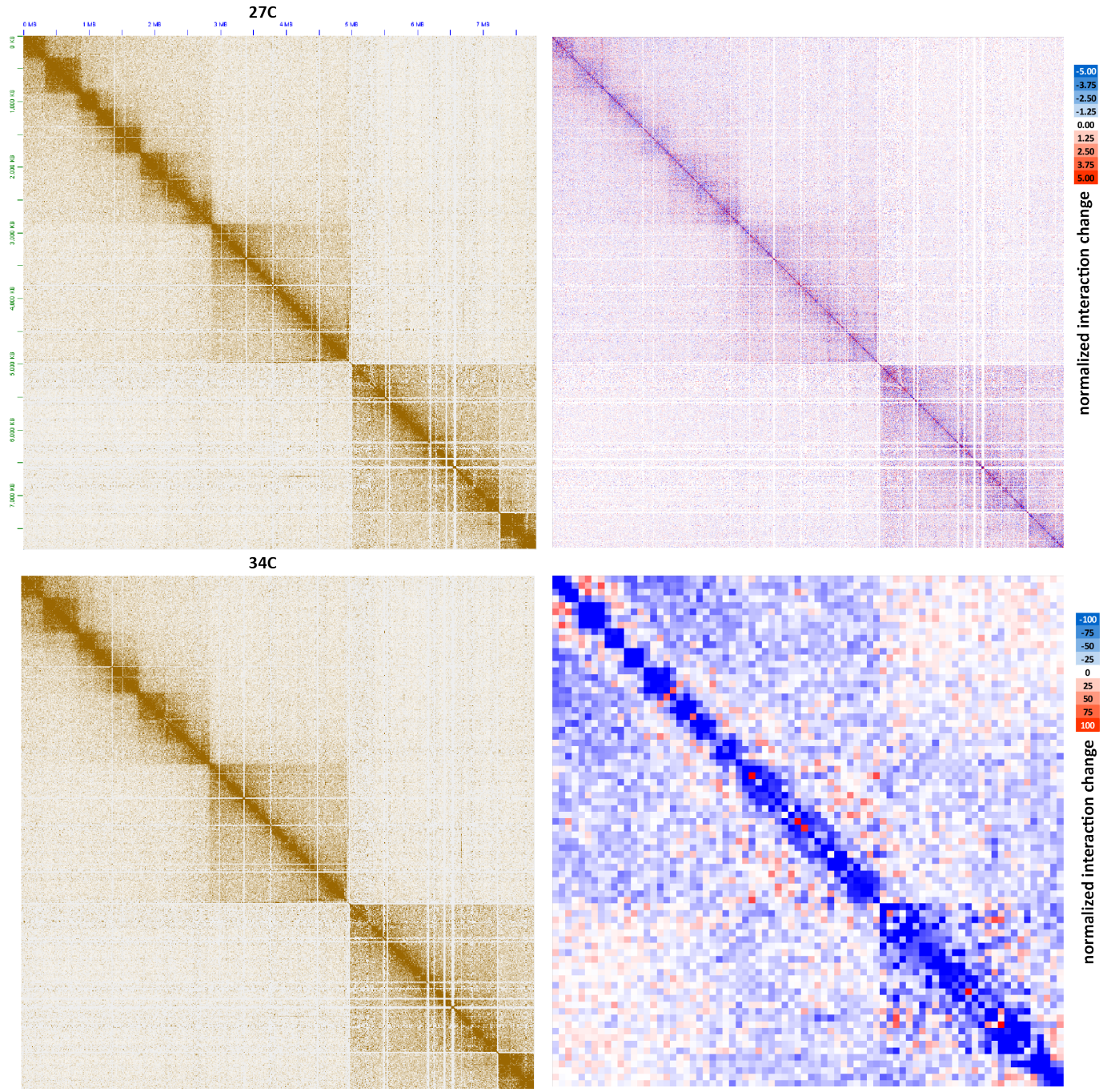

Supplementary Figure 21: Moderate decompaction of dinoTADs upon exposure to elevated temperatures. Shown is pseudochromosome 18 (KR-normalized) and the difference between the KR-normalized Hi-C maps generated from *B. minutum* grown at 34 °C and at 27 °C at 100-kb resolution (lower right) and 5-kb resolution (upper right).

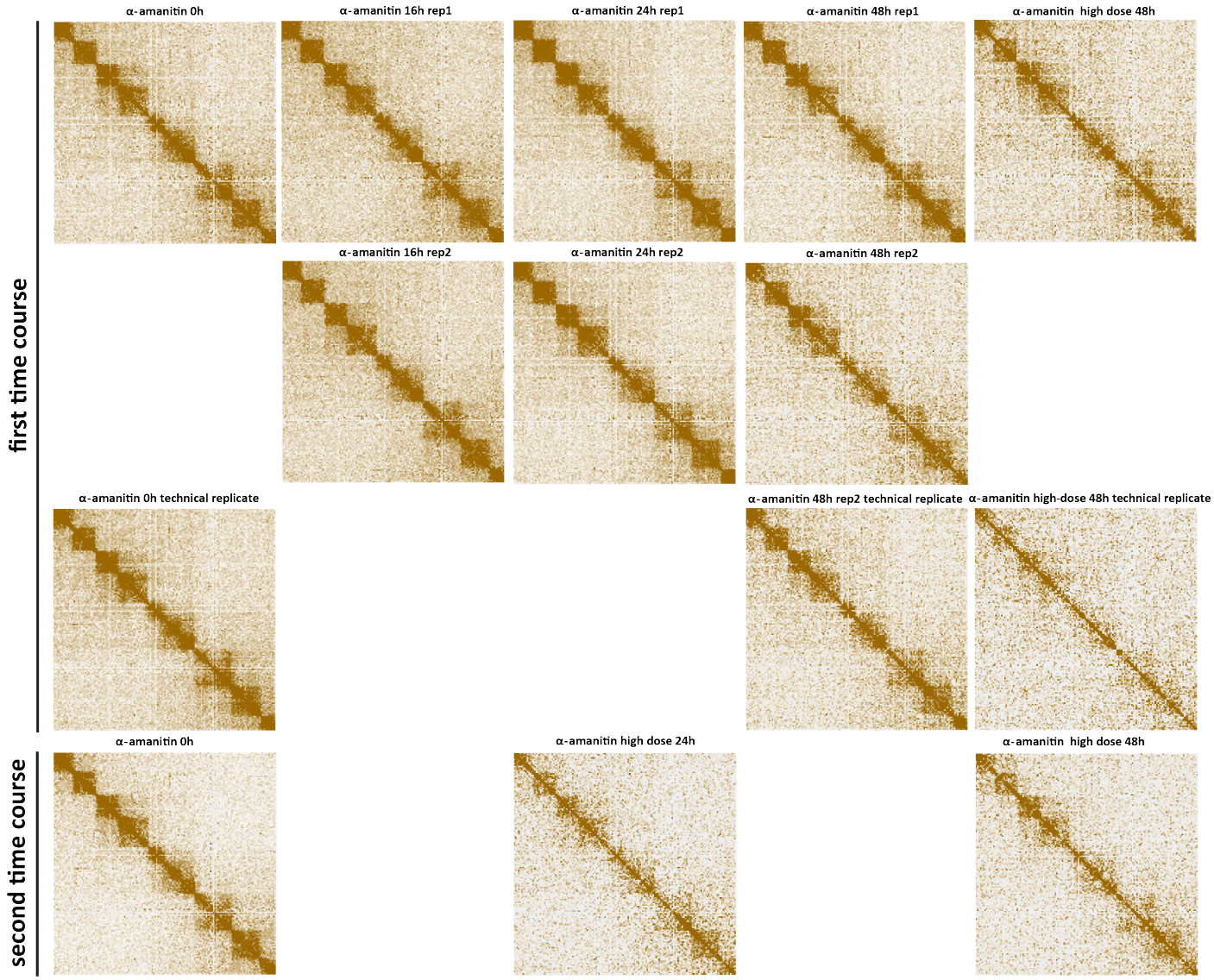

Supplementary Figure 22: Decompaction of dinoTADs upon transcriptional inhibition using α-amanitin. Shown is pseudochromosome 10. Two time courses were carried out following the outline presented in Figure 2B.

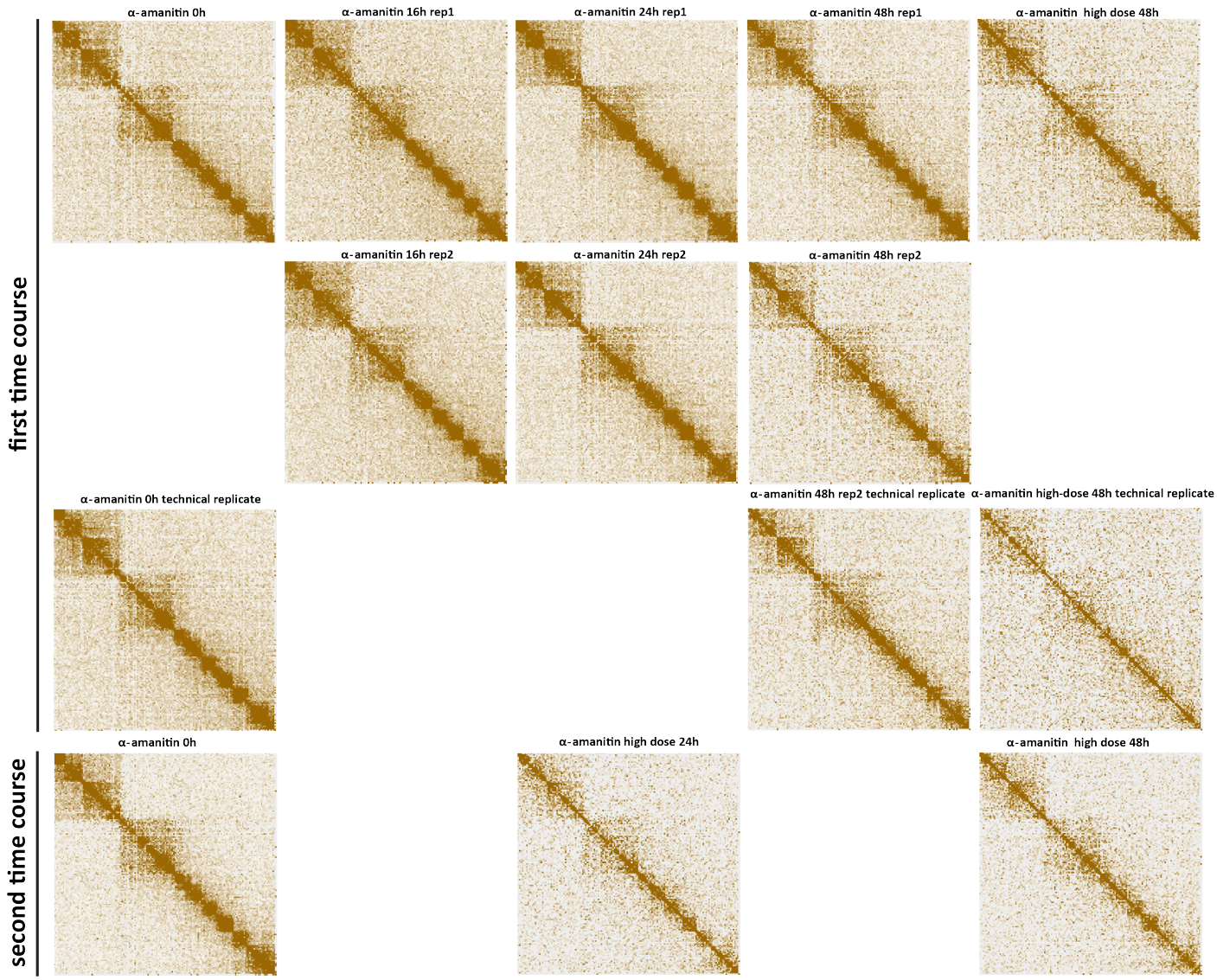

Supplementary Figure 23: Decompaction of dinoTADs upon transcriptional inhibition using α-amanitin. Shown is pseudochromosome 17. Two time courses were carried out following the outline presented in Figure 2B.

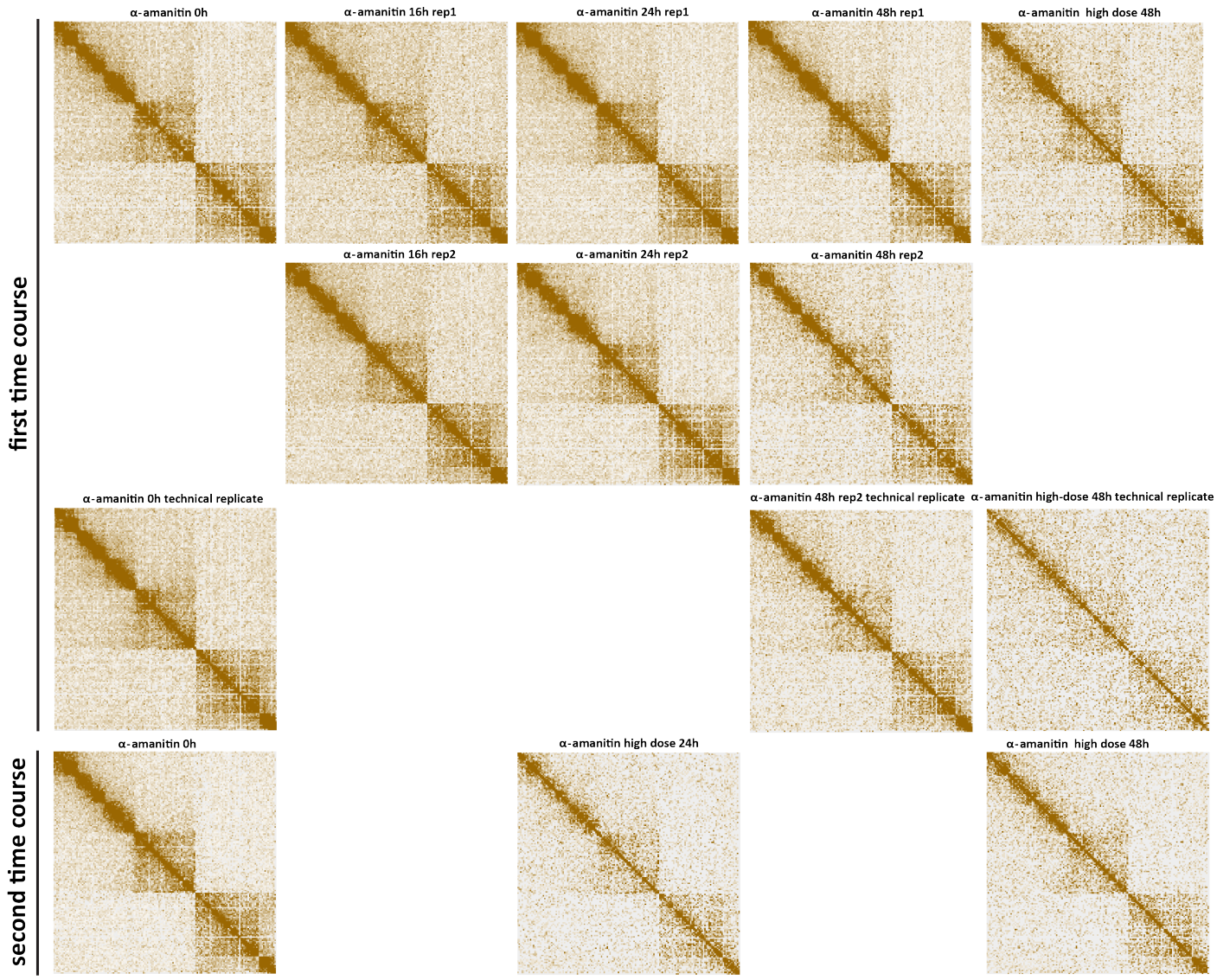

Supplementary Figure 24: Decompaction of dinoTADs upon transcriptional inhibition using α-amanitin. Shown is pseudochromosome 18. Two time courses were carried out following the outline presented in Figure 2B.

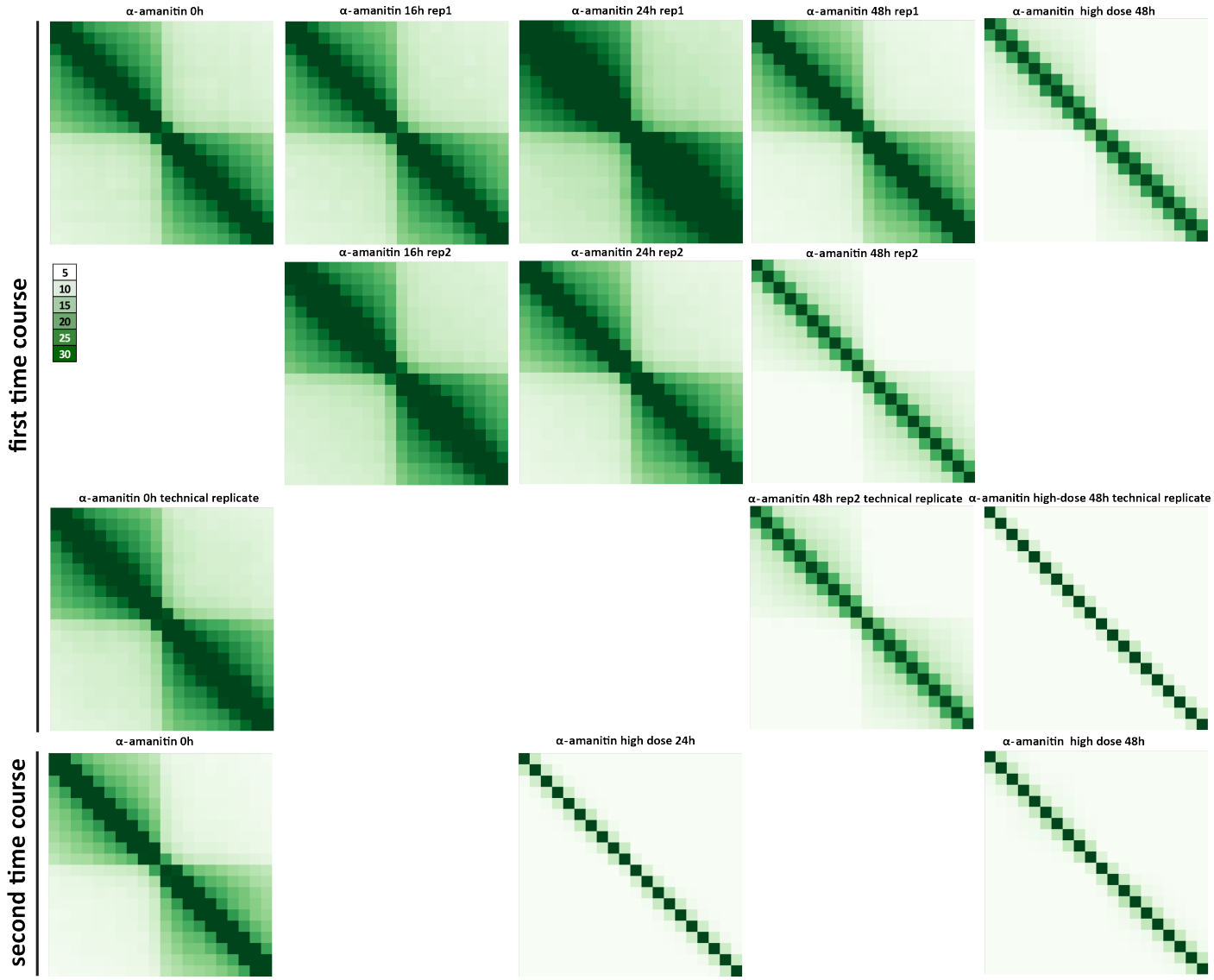

Supplementary Figure 25: Decompaction of dinoTADs upon transcriptional inhibition using α-amanitin. Shown are 50-kb resolution metaplots centered on dinoTAD domain boundaries. Two time courses were carried out following the outline presented in Figure 2B.

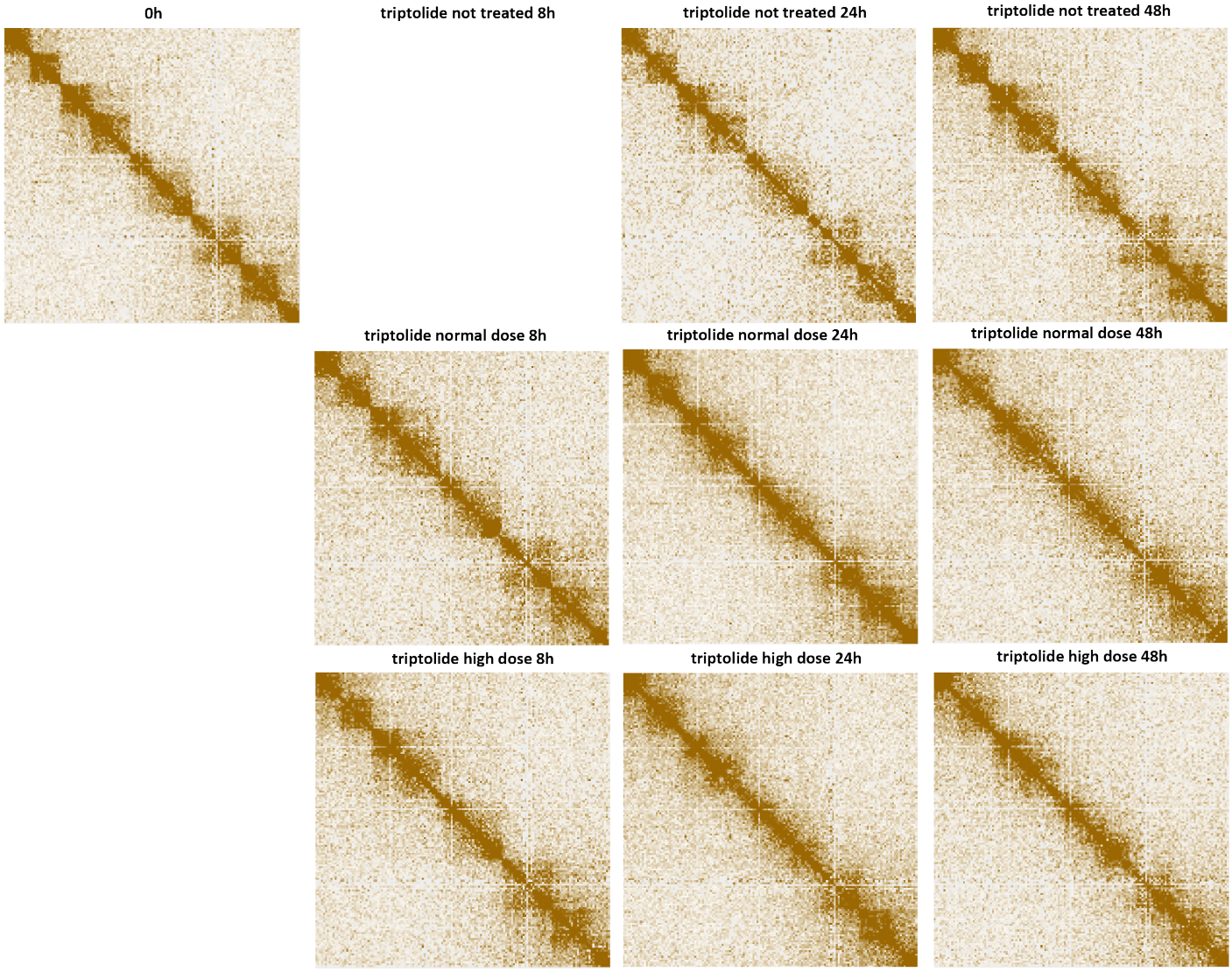

Supplementary Figure 26: Blurring of dinoTAD boundaries upon transcriptional inhibition using triptolide. Shown is pseudochromosome 10. The triptolide time course was carried out following the outline presented in Figure 2B.

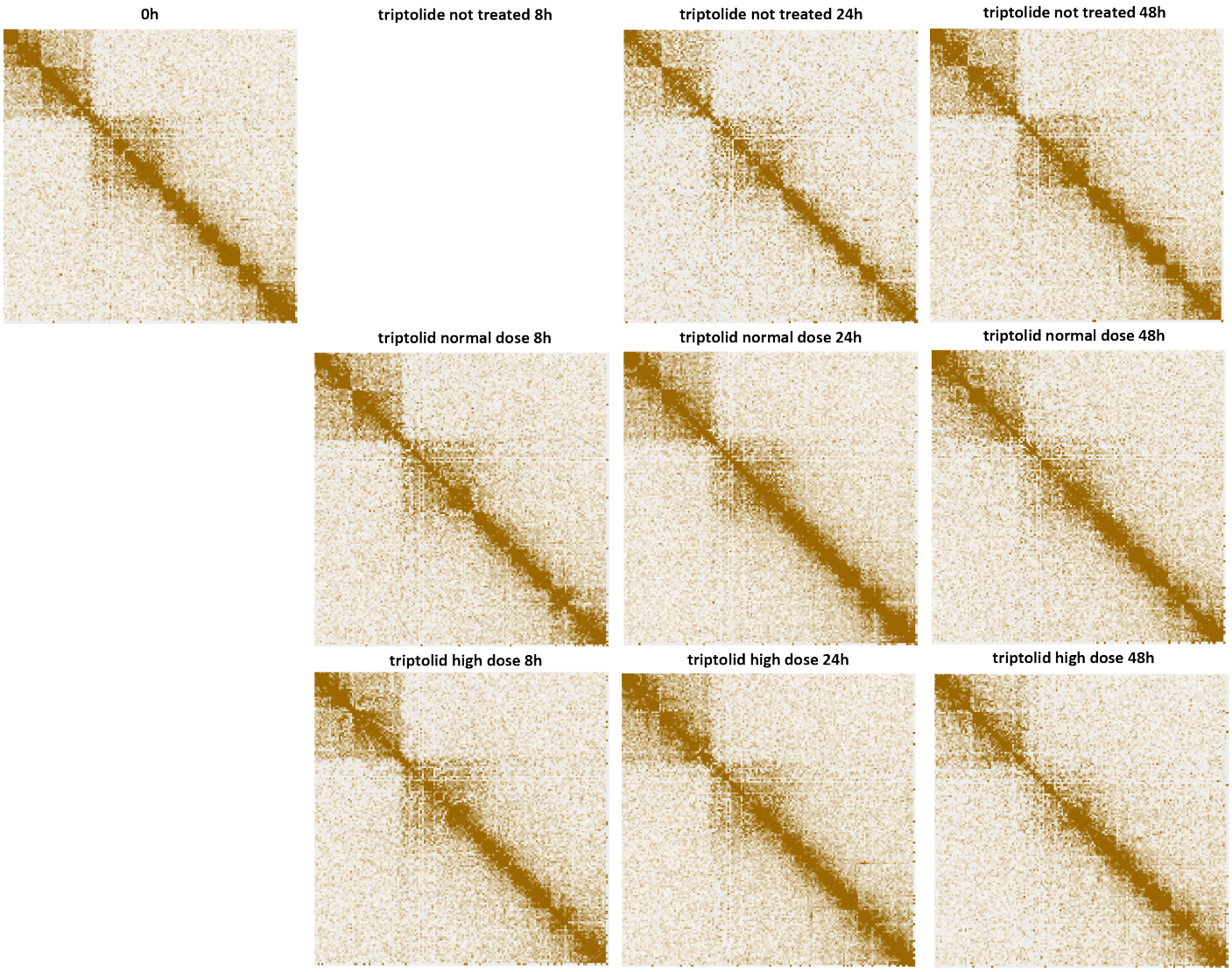

Supplementary Figure 27: Blurring of dinoTAD boundaries upon transcriptional inhibition using triptolide. Shown is pseudochromosome 17. The triptolide time course was carried out following the outline presented in Figure 2B.

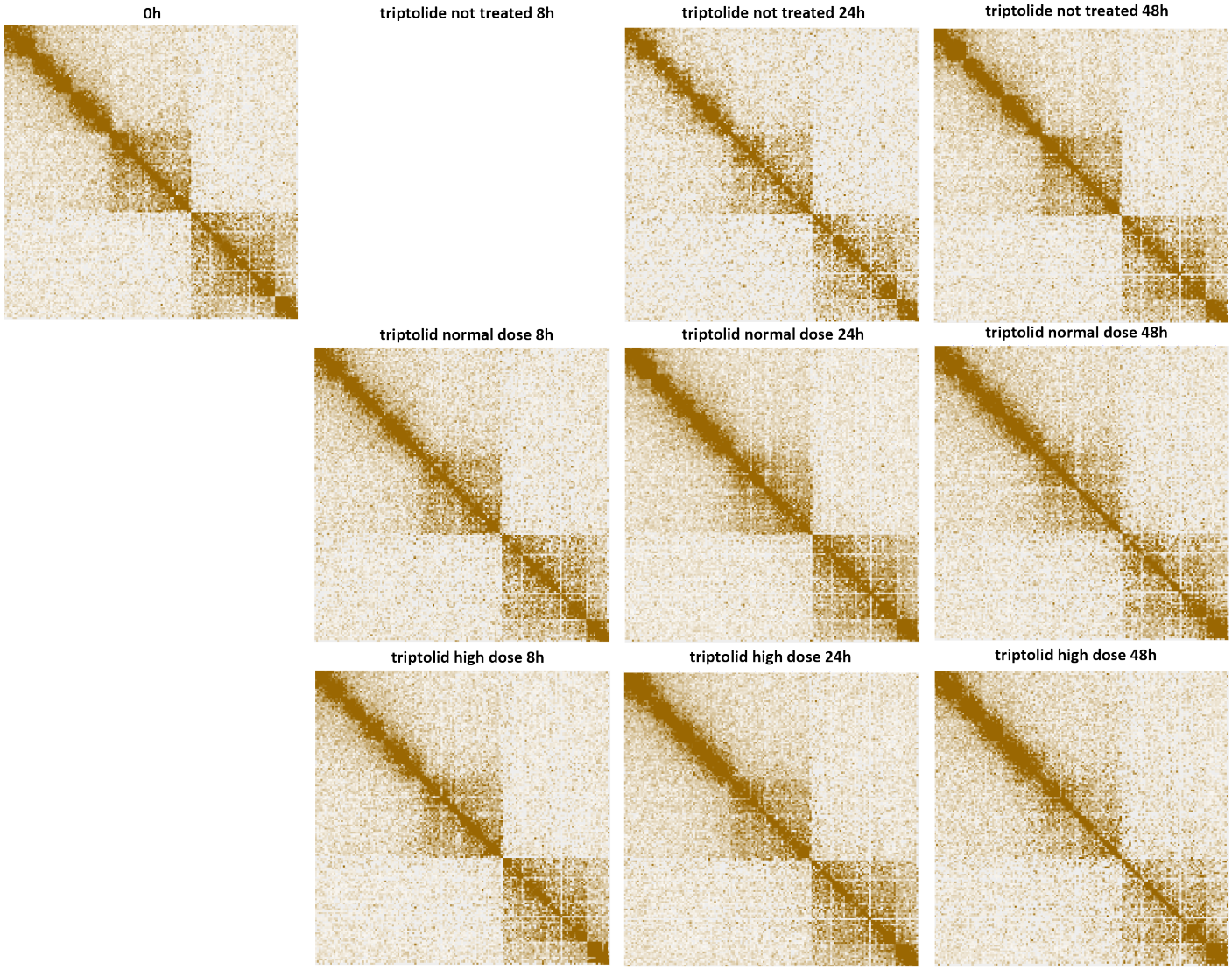

Supplementary Figure 28: Blurring of dinoTAD boundaries upon transcriptional inhibition using triptolide. Shown is pseudochromosome 18. The triptolide time course was carried out following the outline presented in Figure 2B.

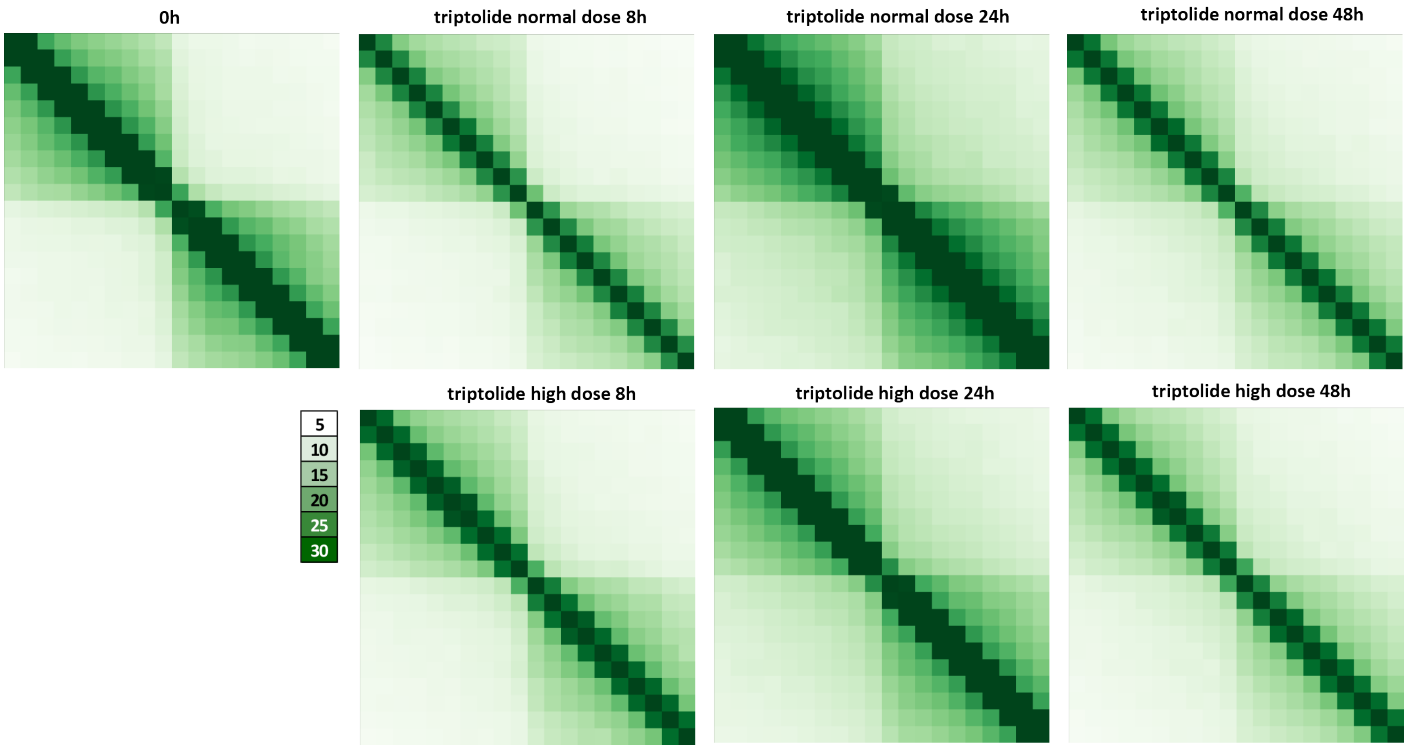

Supplementary Figure 29: Blurring of dinoTAD boundaries upon transcriptional inhibition using triptolide. Shown are 50-kb resolution metaplots centered on dinoTAD domain boundaries. The triptolide time course was carried out following the outline presented in Figure 2B.

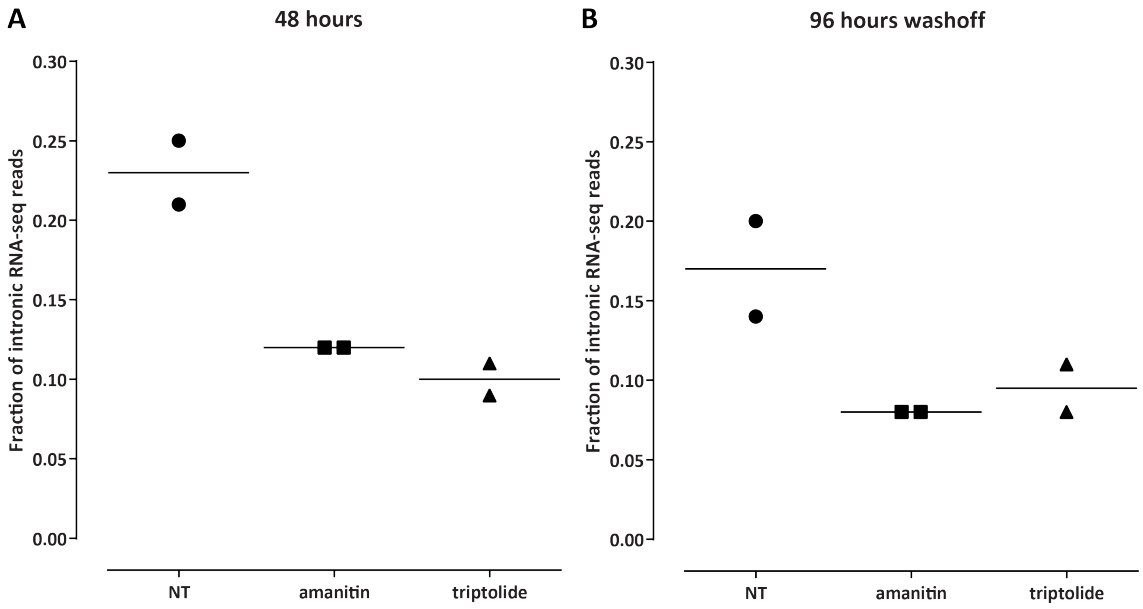

Supplementary Figure 30: Assessment of transcriptional activity upon α-amanitin and triptolide treatment and after withdrawal of the inhibitors. Shown is the fraction of intronic reads in PolyA+ RNA-seq datasets generated from cells treated with the "high" doses of the two drugs or no drug for 48 hours (A) , and at 48 hours later after withdrawing the inhibitor (B; "96 hours washoff"). Note that these samples correspond to the "third time course" shown in Supplementary Figures 32 and 33.

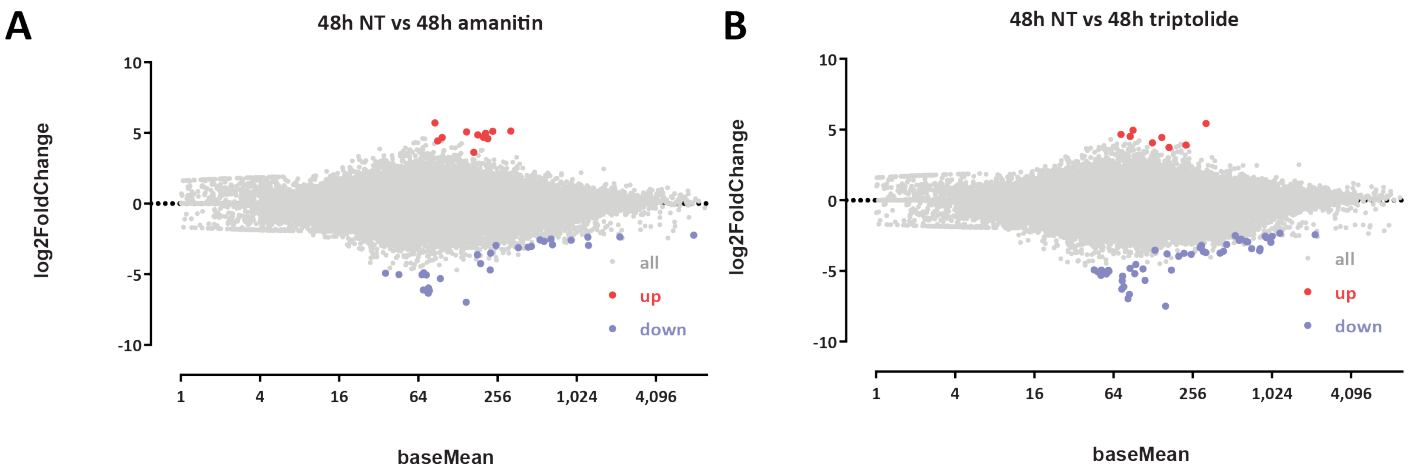

Supplementary Figure 31: Lack of large-scale transcript level changes upon α-amanitin and triptolide treatment. Differential expression was assessed using DESeq2 (see Methods). Number of differential genes: 12 genes up in and 30 genes down in the α-amanitin-treateed relative to the untreated sample; 9 genes up in and 47 genes down in the triptolide-treated relative to the untreated sample. Note that these samples correspond to the "third time course" shown in Supplementary Figures 32 and 33.

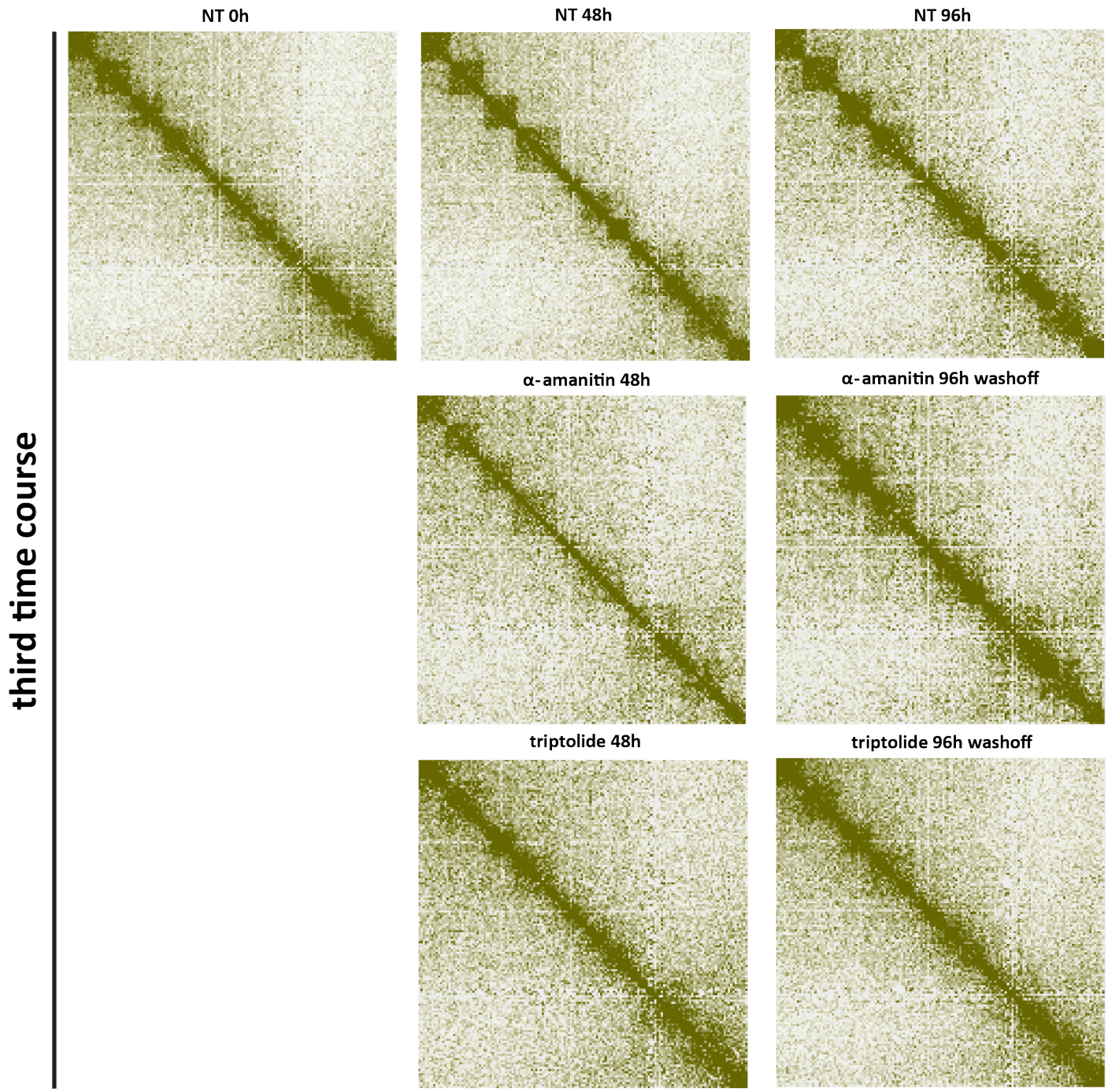

Supplementary Figure 32: Partial restoration of dinoTADs within 48 hours after removal of transcriptional inhibitors. Cells were treated with α-amanitin or triptolide ("high" doses) for 48 hours, then the inhibitors was washed away, and cells were harvested another 48 hours later ("96 hours washoff"). Shown is pseudochromosome 10.

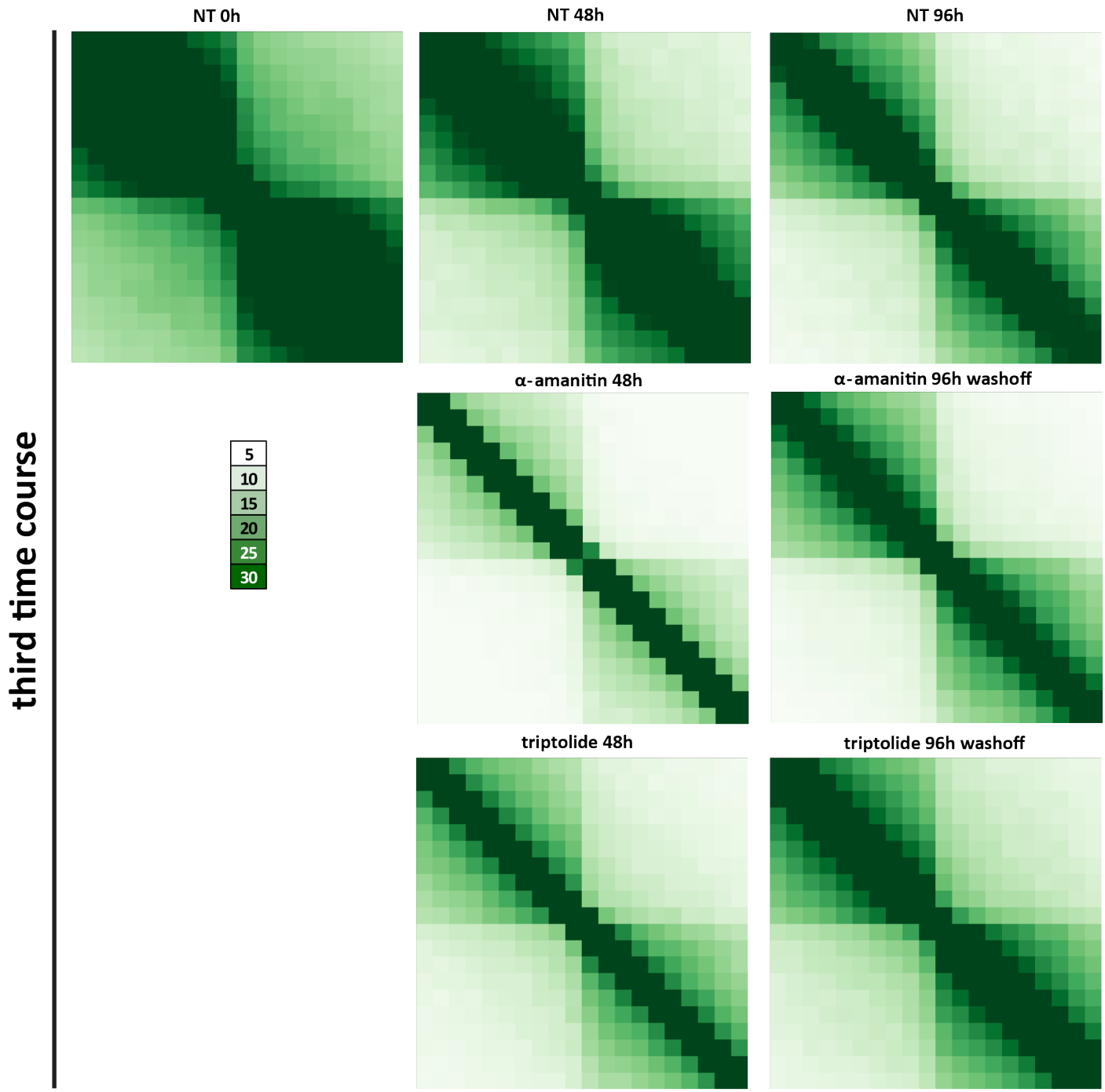

Supplementary Figure 33: Partial restoration of dinoTADs within 48 hours after removal of transcriptional inhibitors. Cells were treated with α-amanitin or triptolide ("high" doses) for 48 hours, then the inhibitors was washed away, and cells were harvested another 48 hours later ("96 hours washoff"). Shown is a metaplot across all dinoTAD boundaries.